Earth Surf. Dynam., 13, 41–70, 2025
https://doi.org/10.5194/esurf-13-41-2025

Earth Surface Dynamics
Open Access
EGU

Massive permafrost rock slide under a warming polythermal glacier deciphered through mechanical modeling (Bliggspitze, Austria)

Felix Pfluger[1], Samuel Weber[2,3], Joseph Steinhauser[1], Christian Zangerl[4], Christine Fey[4], Johannes Fürst[5], and Michael Krautblatter[1]

[1]Landslide Research Group, TUM School of Engineering and Design, Technical University of Munich, Munich, Germany
[2]WSL Institute for Snow and Avalanche Research SLF, Davos Dorf, Switzerland
[3]Climate Change, Extremes and Natural Hazards in Alpine Regions Research Center CERC, Davos Dorf, Switzerland
[4]Institute of Applied Geology, BOKU University, Vienna, Austria
[5]Institut für Geographie, Friedrich-Alexander-Universität Erlangen-Nürnberg, Erlangen, Germany

Correspondence: Felix Pfluger (felix.pfluger@tum.de)

Received: 9 August 2024 – Discussion started: 22 August 2024
Revised: 25 October 2024 – Accepted: 7 November 2024 – Published: 16 January 2025

Abstract. Recent studies have brought to light large amounts of evidence for enhanced rock slope failure from degrading permafrost rock walls. These failures have previously been thought to be subaerial and triggered by thermal heat propagation from rising air temperatures into the exposed rock faces. However, we have neglected the fact that the dividing line between cold and warm basal states of polythermal glaciers has shifted some hundreds of meters upwards at the same time. This means that previously frozen and ice-filled fragmented rock walls under cold glaciers have suddenly and for the first time in thousands of years been exposed to (i) hydrostatic pressures, (ii) warming and degrading ice in fractures, and (iii) rock mechanical degradation in warming rocks. In this paper, we hypothesize that the transition from cold- to warm-based glaciers, a scarcely observed but widespread phenomenon, caused the massive rock slide. To challenge this hypothesis, we investigated the 3.9 to 4.3×10^6 m^3 rock slide at Bliggspitze on 29 June 2007, which detached from a north-exposed, glacier-covered rock slope at 3200 m above sea level. We (a) have analyzed the glacier transition since 1971 using aerial photographs coincident to meteorological data; (b) compared 2013–2016 ground surface temperature measurements to infer permafrost-prone and cold glacier thermal conditions; (c) categorized springs mapped in summer 2001/2012 according to geomorphological features and mineralization; (d) performed electrical resistivity tomography subsequent to failure on the destabilized rock flank in 2009; (e) conducted rock testing in frozen and unfrozen conditions; and (f) modeled the mechanical impact of hydrostatic pressure, degradation of permafrost, and glacier retreat in a universal distinct element code (UDEC). Aerial photos indicate the existence of a cold glacier from 1971–2003 above the failure volume. On the rock face above the failure volume, ground surface temperature measurements demonstrate permafrost-favorable conditions and underpin the presence of former and present cold-based glacier compartments. Since 2003, the warming of the Northern Bliggferner Glacier has been evident in the lower and upper parts. In 2007, subsequent to the warmest January–June period in a 228-year temperature record in the area of Bliggspitze, the glacier opened massive ice crevasses above the later rock slide, causing frequent ice fall. New springs developed in the former permafrost flank, and some were strong enough to cause debris flows. The high mineralization measured at springs at a proximal distance to the failure volume indicates active-layer thaw. The inversion of electrical resistivity tomography revealed thaw that reached several decameters in depth in the collapsed rock mass 2 years after failure. The tensile strength of tested paragneiss rock samples decreased by −40 % from frozen to unfrozen states, which reflects the mechanical degradation of rock

bridges under warming permafrost. In this paper, we demonstrate a new type of rock slope failure mechanism triggered by the uplift of the cold–warm dividing line in polythermal alpine glaciers, a widespread and currently under-explored phenomenon in alpine environments worldwide.

1 Introduction

During the paraglacial transition, geomorphological activity increases in alpine areas worldwide (Gruber and Haeberli, 2007; Ballantyne et al., 2014). Both permafrost degradation and glacier retreat alter thermal and hydrological regimes of rock slopes, challenging their mechanical stability (McColl and Draebing, 2019; Grämiger et al., 2020). Although the detachment areas of high-volume rock slope failures in the mountain cryosphere are often in remote locations, the cascading effects of the propagating mass movement can be severe, causing casualties and damage to infrastructure (Walter et al., 2020; Shugar et al., 2021; Geertsema et al., 2022). With the observed warming of permafrost (Biskaborn et al., 2019) and volume loss of glaciers in recent decades (Hugonnet et al., 2021), hazard source areas are expanding to higher elevations (Ballantyne, 2002; Huggel et al., 2012), potentially reactivating dormant rock slopes.

In contrast to the relatively high frequency of low-volume failure events situated in zones of potential permafrost in the Swiss Alps, the rare events of high-volume rock slope failures $> 10\,000\,\mathrm{m}^3$ appear to not follow the observed pattern of seasonality (Phillips et al., 2017). Due to the complexity of large rock slope failures, their often remote alpine locations with challenging accessibility that result in limited available data, and the absence of a clear seasonal pattern, predicting such failures in permafrost regions is challenging (Huggel et al., 2008; Svennevig et al., 2020).

Investigating the timing of rock slope failures in Scotland and northwestern Ireland in relation to deglaciation, Ballantyne et al. (2014) found that 95 % of the analyzed failures occurred within approximately 5400 years after deglaciation, with peak activity occurring between 1600 and 1700 years post-deglaciation. They suggests that glacier unloading and seismic activity were the primary triggers. Similarly, Hermanns et al. (2017) identified a time cluster of rock avalanche deposits in Norway originating from the first millennium after deglaciation and a second cluster during the Holocene climatic optimum. Studying rock slope failures in the European Alps, Prager et al. (2008) noted a time cluster of events several thousand years after ice withdrawal. These failures, occurring several thousand years after deglaciation, are hypothesized to have been prepared by glacial cycles and finally triggered with a time lag relative to the Last Glacial Maximum (LGM), accounting for the loss of permafrost (McColl, 2012; Krautblatter et al., 2013). Permafrost in the Late Glacial has suppressed crack propagation and postponed rock slope failures to the Early Holocene (Krautblatter and Leith, 2015).

Over long timescales, glaciation cycles predispose rock slopes to failure by (i) over-steepening of valley flanks as a result of glacial erosion (Holm et al., 2004; Mitchell and Montgomery, 2006); (ii) glacier advance and retreat causing mechanical stress release or increase to the bedrock, resulting in crack initiation and propagation in the underlying bedrock (Leith et al., 2014; Grämiger et al., 2017) or even in first-time slope failure by reaching displacements of several decimeters to meters (Fischer et al., 2010; Rechberger and Zangerl, 2022); (iii) glacial hydrology exerting hydromechanical stresses in fractures (Grämiger et al., 2020); and (iv) sudden change in thermal regime during paraglacial transitions exerting thermomechanical stresses to the rock mass (Grämiger et al., 2018).

In contrast, permafrost impacts the strength of rock slopes and intact rock properties, contingent upon its thermal state and distribution. The observation of ice-filled joints at failure scarps in permafrost rock (Gruber and Haeberli, 2007; Zangerl et al., 2019; Krautblatter et al., 2024) and its mechanical relevance were pointed out by laboratory studies on shear tests (Davies et al., 2001; Günzel, 2008; Krautblatter et al., 2013; Han et al., 2023). Warming permafrost is found to be a key factor in preconditioning rock slides along defined shear planes with ice-infillings. While warming, the shear strength of ice-filled joints decreases by 17.2 % for each degree Celsius increase in temperature within the range of -4 to $-0.5\,^{\circ}\mathrm{C}$ at an applied normal load of 0.8 MPa according to Mamot et al. (2018). The shear strength of ice-filled joints, relevant for the stability of fractured rock mass, decreases distinctly while warming, and intact rock properties also indicate similar behavior. As temperatures rise towards the freezing point, p-wave velocities (Draebing and Krautblatter, 2012) and electrical conductivity (Krautblatter et al., 2010) experience a distinct drop before reaching a plateau at temperatures above $0\,^{\circ}\mathrm{C}$. Tensile strength decreased for relatively soft rock types such as sandstone and limestone by 67 % and 61 %, respectively, and for hard rock types such as granite by 6 % when comparing mean results of saturated intact rock samples tested at -2.5 and $+1.65\,^{\circ}\mathrm{C}$. Uniaxial compressive strength decreased for sandstone and limestone by 35 % and 42 %, respectively, and for hard rock types such as granite by 0.5 % when comparing mean results of saturated intact rock samples tested at -2 and $+1.5\,^{\circ}\mathrm{C}$ (Mellor, 1973).

Permafrost acts as an impermeable hydrogeologic layer by sealing the rock matrix and fractures. The advective trans-

fer of heat conveyed by percolating water substantially accelerates permafrost degradation in comparison to conductive heat flow alone. Favored by complex alpine topography, this process leads to the formation of deep thaw corridors along fractures, intersecting the permafrost body and enabling the buildup of high transient hydrostatic pressures (Hasler et al., 2011; Magnin and Josnin, 2021). During periods of excess meltwater or precipitation, the transient rise in hydrostatic pressure is likely to destabilize greater slope volumes than rock and ice mechanical degradation under conductive warming alone (Gruber and Haeberli, 2007; Draebing et al., 2014).

To date, the impact of glacier activity and permafrost degradation on rock slope mechanics has been the subject of separate studies. However, the interactions between both have not been considered. The Bliggspitze (Austria) rock slide is situated in alpine permafrost and appears to be strongly linked to the activity of the Northern Bliggferner Glacier covering the slope before the first-time formation of the rock slide. The geology and kinematics of the Bliggspitze rock slide have been investigated in detail by Zangerl et al. (2019), but the processes leading to the rock slide remain unexplored. This paper focuses on the coupled effects of the glacier's thermal regime on permafrost and hydrogeology and their mechanical implications, with the aim of investigating the processes destabilizing the 3.9 to 4.3×10^6 m^3, deep-seated rock slide at Bliggspitze in June 2007.

In this paper, we address the following three principal questions.

1. Can we decipher a cold-to-warm glacier transition using geophysics, temperature, and hydrological data?
2. How does the interaction of polythermal glaciers and bedrock permafrost destabilize rock slopes under climate change?
3. How does the change in thermal state affect rock slope mechanics using tensile strength as a proxy?

The study design is structured into three sections, each of which corresponds to the order of the research questions. The third section builds on the results presented in the previous sections. First, we investigate the evolution of the Northern Bliggferner Glacier in the decades before the first-time formation of the Bliggspitze rock slide, the permafrost conditions based on data recorded in the years after, and field observations and meteo records in the weeks immediately before the event. Secondly, we conducted tensile strength tests under frozen and unfrozen conditions and varying foliation orientation of paragneiss rock to constrain assumptions for the subsequent modeling study. Third, we conceptualized a mechanical model framework for the case of the Bliggspitze rock slide. We hypothesize that the cold–warm dividing line of the glacier base is shifting to higher elevations under climate warming, affecting permafrost and hydrogeologic conditions. We investigate (i) the structural predisposition of the rock slope and analyze the impact of cryospheric forcings such as (ii) glacier unloading, (iii) permafrost degradation, and (iv) transient hydrostatic water pressure on rock slope mechanics by using a distinct element model.

To distinguish between the phases of slope deformation, we define the pre-failure, sudden-failure, and post-failure stages as follows: the pre-failure stage spans months, years, or even decades, during which the rock slope undergoes initial deformation, typically at a rate of millimeters to centimeters per year, before experiencing a distinct acceleration. The sudden-failure stage marks the first-time formation of the Bliggspitze rock slide in June 2007, coinciding with the creation of the basal shear zone at the head scarp. This period is characterized by a sharp increase in velocity, reaching from meters up to several decameters per day, and associated activity in the hours and days surrounding the event. The post-failure stage involves the ongoing deformation of the displaced rock mass in the months and years following the first-time formation of the rock slide (Leroueil et al., 1996).

2 Bliggspitze field site

Bliggspitze summit (3453 m a.s.l., 46°55′5″ N, 10°47′10″ E – WGS84) is located on the Kaunergrat ridge, which runs north–south and separates the Pitztal and Kaunertal in Tyrol, Austria (for the exact location, see the map in Fig. 1). Glaciers encircle the summit. The Eiskastenferner Glacier is situated to the east, while the Northern Bliggferner Glacier and Southern Bliggferner Glacier are located to the west. The deep-seated rock slide occurred on the north-facing slope of Bliggspitze, predominantly covered by the Northern Bliggferner Glacier (Fig. 2a). A volume in the range of 3.9 to 4.3×10^6 m^3 of glacier ice and rock mass was mobilized by the rock slide on 29 June 2007. Concomitant to the primary sliding process, secondary processes such as rock falls, combined rock–ice avalanches, and debris flows have been observed hours and days before and after the event. The first-time formation of the Bliggspitze rock slide caused it to disintegrate into individual slabs and created a continuous basal shear zone, as indicated by the shear offset of the head scarp. Post-failure activity was evident in the months and years after the first-time formation of the rock slide. As the movement of the fragmented rock mass above the basal shear zone decelerated, various types of rapid movements with small volumes, such as rock falls, debris avalanches, and debris flows, and moderate movements, such as rock and soil slides, originated from the fragmented rock mass in the years after (process terminology after Cruden and Varnes, 1996).

The outlines of the Northern Bliggferner Glacier remained relatively stable between 1969 and 2006, as shown in Fig. 1. The Northern Bliggferner Glacier was divided into two sections, an upper and a lower one, with a substantial rock outcrop in the middle since at least 1969 (Fig. 2a). By comparing the glacier from historic maps of 1946 and airborne laser

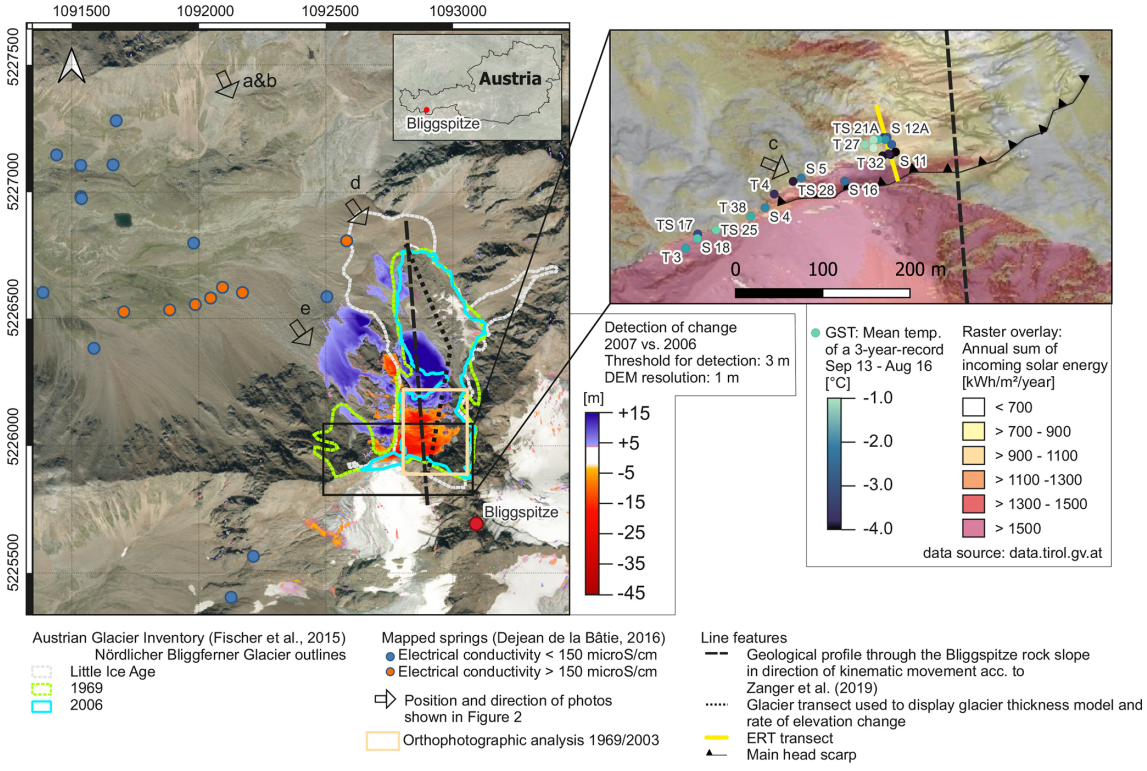

Figure 1. Overview of the study site, illustrating the dimensions of the affected rock slope; historic glacier outlines; the position and results of measurements, including ground surface temperatures and electrical conductivity of springs; and profile sections of electrical resistivity tomography through the rock slide. The left map shows Würmtal, including the peak of Bliggspitze at the lower right (3453 m a.s.l.). The right map is a detailed zoomed-in view of the head scarp located at 3270 m a.s.l. Glacier outlines are given for the Northern Bliggferner Glacier. The Southern Bliggferner Glacier is situated to the west of the summit of Bliggspitze, while the Eiskastenferner Glacier is located to the east. The left base map is from Orthophoto (August 2015), while the right slope map is from the post-failure stage (2007). The DEM of 2006 and 2007 used for change detection is provided by Land Tirol (https://www.tirol.gv.at/data/), and the Coordinate Reference System of the map is as follows: EPSG:32631 – WGS 84/UTM zone 31N.

scanning data from 2006, it was found that the Northern Bliggferner Glacier has experienced a significant loss in thickness, particularly in the lower section and slightly above the rock outcrop, with a reduction of several decameters (Zangerl et al., 2019).

The Bliggspitze rock slope is situated at the southern limb of a tectonic synform, with foliation of the paragneissic rock running sub-parallel to the slope. The rock mass is characterized by four distinct joint sets with spacing in the range of 0.2–0.6 m and steeply dipping fault zones at the top and middle sections of the slope (Dejean de la Bâtie, 2016). The head scarp was created by shearing off a prominent fault zone at 3270 m a.s.l., resulting in a discrete shear offset of 40 m (Fig. 2b and c). The rock mass affected by the rock slide extends to an elevation of about 2900 m a.s.l., most likely following a curved basal shear zone or rupture surface (for the structural geological profile, see Fig. 3a). The existing fault zones were found to be crucial in the predisposition of the Bliggspitze rock slide. The fault zones at the Bliggspitze rock slopes can be characterized as soil-like brittle tectonic fault zones, with a high proportion of sheet silicate minerals (mica group 20 % – −30 %, chlorite group 10 %–20 %), yielding residual friction angles within the range of 25.7–28.9°, as determined in laboratory tests (Strauhal et al., 2017). A comprehensive geological and kinematic model of the Bliggspitze rock slide can be found in the publication of Zangerl et al. (2019).

3 Methodological approach

3.1 Field methods and data for pre-failure analysis of the Bliggspitze rock slide

The chronology preceding the formation of the Bliggspitze rock slide was analyzed by utilizing climate, meteorological, and discharge data and examining the related events that occurred in the years and weeks before the rock slide (Table 1). Tables 1 and 2 summarize time series and spatial data used to infer glacier evolution and permafrost conditions. Figure 1 shows an overview of the study site, including the extent of the rock slide and past glacial outlines, and compiles the po-

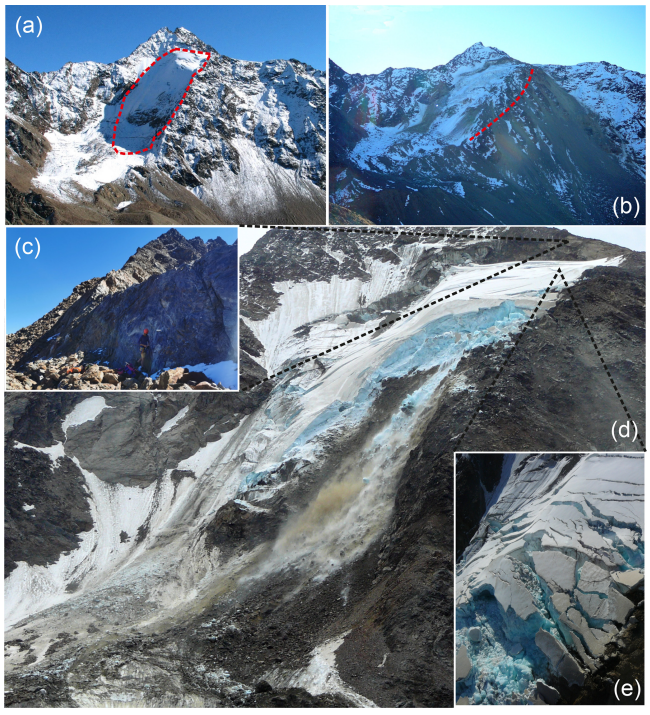

Figure 2. Photographs of the Bliggspitze rock slope taken of the pre-, sudden-, and post-failure stage. **(a)** An overview from the northwest with the Northern Bliggferner Glacier in the center, where the glacier is divided into an upper and lower section by the rock outcrop in the middle (pre-failure stage in summer 2003). **(b)** The post-failure stage indicated by the fragmented glacier at the top and the sedimentation of debris at the lower part of the glacier (October 2007), where the inferred shear plane is illustrated with a dashed red line in the figure. Debris flows altered the west-facing slope in the years and days prior to the first-time formation of the rock slide in June 2007. **(c)** The basal shear zone at the head scarp with polished slickenside and the fragmented rock mass underneath. **(d)** Rock and ice falls (secondary processes related to the rock slide are from the sudden-failure stage). **(e)** The widening of crevasses and fragmentation of glacier ice at the upper section favoring meltwater infiltration into bedrock (sudden-failure stage). Dashed black lines indicate the location of more detailed and zoomed-in views. The photographs were kindly provided by Michael Krautblatter and Gunther Heißel. The position and direction of the photographs are indicated in Fig. 1, with all photos facing approximately SE.

sition and results of investigations on permafrost at the site in a map.

Glacier changes were analyzed by mapping visual changes in historic orthophotos. In addition, we compared the rate of annual glacier elevation change for given periods during pre-, sudden-, and post-failure stage. For the pre- and post-failure stage, we calculated the rate of annual glacier elevation change via DEM-based raster calculation (1969–2000, 30 m resolution; 2007–2017, 1 m resolution; see Table 2). For the sudden-failure stage, we refer to the published dataset by Sommer et al. (2020) (2000–2012, 30 m resolution).

Permafrost conditions were inferred by ground surface temperature (GST) and electrical resistivity tomography (ERT) in the area below the head scarp (for the location of the profile, see Fig. 1), the measured mineralization of springs, and field observations such as ice-filled fractures.

For the recording of GST, 22 temperature loggers were placed in open fractures a few decimeters below the surface within the failed rock mass at an elevation of 3200 ±20 m a.s.l. The loggers were covered with loose debris to avoid direct contact with snow cover and exposure to solar radiation. The applied HOBO U22-001 loggers recorded temperature every 2 h from 2 September 2013 to 31 August 2016. We used daily standard deviation as a proxy to detect snow cover according to Haberkorn et al. (2015) and Draebing et al. (2022). Daily standard deviation > 0.5°C indicates snow-free conditions, whereas daily standard deviation < 0.5°C indicates presence of snow cover that buffers air temperature and incoming solar radiation signals. Additionally, a daily standard deviation < 0.001 °C was used as a threshold to detect the zero curtain. The data were initially published by Zangerl et al. (2019) and subsequently reanalyzed in the present study.

The ERT was conducted on 12 August 2009, 2 years after the first-time formation of the Bliggspitze rock slide. For the ERT survey, we used a Wenner array to measure 190 data points with a profile length of 100 m and electrode spacing of 2.5 m. Out of 190 data points, 155 were successfully coupled to the ground and were used for the inversion process with the software RES2DINV-4.10.3 (Loke and Barker, 1996). We conducted inversion under robust data constraint (cutoff factor: 0.005) for a refined model with a cell width of half the unit spacing. As the measured data contained considerable noise, we tested the inversion on a reduced dataset after eliminating measured data points that do not correlate well with the modeled apparent resistivity values. By fitting the model to 128 instead of 155 data points, we could essentially improve the root-mean-square error (RMSE) to a value of 9.4 Ωm after the seventh iteration of the inversion.

We reprocessed data of 32 springs mapped in the area related to the Northern Bliggferner Glacier, Southern Bliggferner Glacier, and Eiskastenferner Glacier in summer 2011 and 2012 to potentially detect water originating from permafrost or glacier melt as a source (original data derived from Dejean de la Bâtie, 2016). Therefore, we classified springs according to the geomorphological forms in their vicinity by the use of orthophotos and digital elevation models and categorized the measured values of electrical conductivity into two groups separated by a threshold of 150×10^{-6} S cm^{-1}.

3.2 Laboratory experiments under frozen and unfrozen conditions

We conducted pseudo-Brazilian tests on intact rock samples under saturated, unfrozen, and frozen conditions and vary-

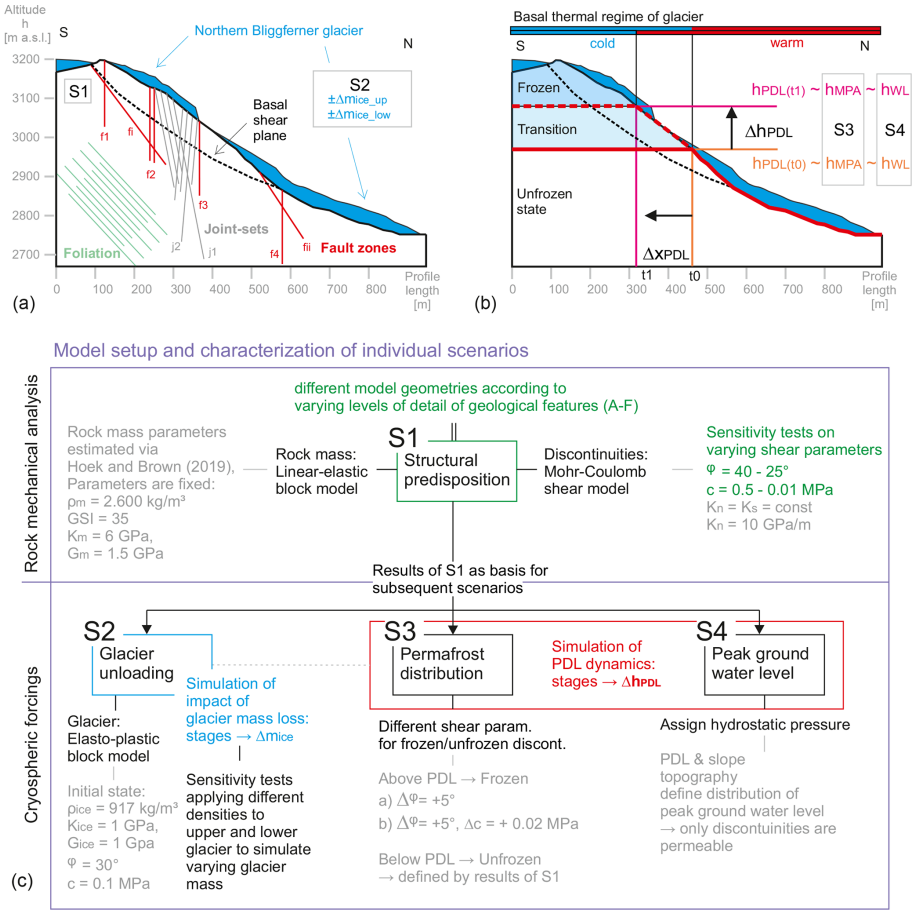

Figure 3. Conceptual scenarios S1 to S4 for investigating rock slope mechanics and interdependencies with environmental forcings in a UDEC model. **(a)** Two-dimensional cross-section for the Bliggspitze rock slide, including geological features and glacier extents of upper and lower sections of the Northern Bliggferner Glacier. **(b)** The polythermal dividing line (PDL) marks the border between cold and warm glacier bases in polythermal glaciers. The PDL poses implications on permafrost and water table within the rock mass. The elevation of PDL h_{PDL} at its current state is equal to the mountain permafrost altitude h_{MPA} and the possible peak groundwater level h_{WL}. **(c)** Description of the UDEC model setup and parameters for simulating the individual scenarios. The following abbreviations apply to S1: ρ_{m} is the density of rock mass, GSI is the Geological Strength Index, K_{m} is the bulk modulus of rock mass, G_{m} is the shear modulus of rock mass, θ is the joint friction angle, c is the joint cohesion, K_{n} is the joint normal stiffness, and K_{s} is the joint shear stiffness. The following abbreviations apply to S2: m_{ice} is the mass of glacier ice ($m_{\mathrm{iceup/low}}$ refers to the distinctly modeled ice bodies located at the upper or lower part of the slope), ρ_{ice} is the density of glacier ice, K_{ice} is the bulk modulus of glacier ice, G_{ice} shear modulus of glacier ice, ϕ is the internal friction angle of glacier ice, and c is the cohesion of glacier ice.

ing foliation orientation. Several decimeter-thick blocks of foliated paragneiss (the same lithologic unit as at Bliggspitze study site) were collected at rock outcrops next to the road along the "Kaunertaler-Gletscher Straße" at three different sites at elevations between 2000 and 2600 m a.s.l.

In the lab, we prepared cylinders 50 mm in diameter and 25 mm in length, maintaining a diameter–length ratio of 2 : 1, as suggested by Lepique (2008). Samples were prepared to be tested with angles of 0, 20, 45, and 90° between foliation and direction of the applied force. All samples were saturated at atmospheric pressure for 24 h until reaching constant mass (DIN-EN-13755:2008-08, 2008) and wrapped in a plastic layer to prevent dehydration. Half of the samples were frozen until reaching a constant temperature of −10 °C and tested under the ambient temperature of 4 ± 1 °C. The other half was kept and tested at room temperature (20 ± 1 °C). To keep the ambient thermal influence on frozen samples while testing as low as possible, samples were removed from the freezer immediately before testing and insulated with styrofoam. They were only exposed to ambient temperature during the tests. To keep track of the warming of the samples, we measured surface temperature and core temperature for specified samples. The core temperature measured at the center of gravity of insulated samples dropped from −10 to −6.8 °C at 5 min after removal from the freezer at no load applied.

Table 1. Meteorological and hydrological time series used to characterize pre- and post-failure conditions.

Time series	Parameters	Observation period	Measurement interval	Location	Source
Histalp dataset 5×5 min grid cell	T	1780–2014	monthly	Würmtal (mid of cell) 2236 m a.s.l.	HISTALP dataset accessible via https://www.zamg.ac.at/histalp (last access: 7 January 2025); Chimani et al. (2013)
Spartacus dataset 1×1 km grid cell	T_{max}, T_{min}, PPT	1961–2022	daily	Southern Bliggferner Glacier (mid of cell)	SPARTACUS dataset accessible via GeoSphere Austria (2023); Hiebl and Frei (2016, 2018)
Hydrology of Vernagt basin	Q, T, elect. conductivity	2007	10 min	8 km distance to site, 2640 m a.s.l.	Escher-Vetter et al. (2014)
Pitztal Glacier meteo station	T	2013–2016	hourly	8 km distance to site, 2863.9 m a.s.l.	GeoSphere Austria (2023); station ID: 17315
Brunnenkogel meteo station	T	2013–2016	hourly	6 km distance to site, 3437 m a.s.l.	GeoSphere Austria (2023); station ID: 173200
Ground surface temperature (GST) measurements	T	hydrological years 2013–2016	2 h	at site, 3200 ± 20 m a.s.l.	Zangerl et al. (2019)

Abbreviations are as follows: T is for temperature, $T_{max/min}$ is for daily peak temperature, PPT is for daily precipitation sum, and Q is for water discharge.

Table 2. Spatial data used to characterize the cryosphere at the site.

Spatial data	Year	File type or resolution	Source
Glacier outlines	LIA, 1969, 1997, 2006	shapefile	Austrian Glacier Inventory; Fischer et al. (2015)
Digital elevation models	2006, 2007, 2017	1 m	Land Tirol – https://www.tirol.gv.at/data/
	2000	30 m	SRTM, Farr et al. (2007)
	1969	30 m	DHM69, Lambrecht and Kuhn (2007)
Glacier thickness models	1970, 2003	30 m	Sommer et al. (2023)
Rate of elevation change of the glacier	2000–2012	30 m	Sommer et al. (2020)
Orthophotos	1969, 2003, 2007, 2009, 2010	0.2–0.25 m	Land Tirol – https://www.tirol.gv.at/data/
Annual sum of incoming solar energy	2013/2014	1 m	Land Tirol – https://www.tirol.gv.at/data/
Mapping of springs and measurement of electrical conductivity	2011, 2012	point file	Dejean de la Bâtie (2016)

All links in this table were accessed on 1 January 2025.

Tensile strength was measured and calculated according to Lepique (2008) with modifications made to the measurement device, resulting in the designation pseudo-Brazilian test (pBZT). Instead of using the recommended testing machine that allows for a continuous increase in load, we employed a manually operated portable point load test apparatus developed by Wille Geotechnik, which is utilized for point load tests. The device has a force gauge to determine the breaking force and was modified by substituting the cones with bridges to change the load type from point load to

strip load. As the manual operating device was transportable, we set it up in a room with a constant ambient temperature of 4–6 °C to keep external thermal influences on frozen samples while testing low. The test duration was limited to a maximum of 3 min. For testing, the cylindrical samples were mounted horizontally and fixed between the opposing bridges contacting the lateral surface. We rotated the samples along the cylindrical axis to test force application on different orientations of the foliation. Brazilian tests are typically conducted using a constant strain rate. In our setup, we opted for a manually operated device that applies force through human power, which resembles a constant stress test. To ensure equal test conditions for all samples, tests were conducted by the same person, with attention paid to increasing the load continuously and consistently. Additional tests ($n = 8$) were conducted to compare the manually operated pBZT procedure with the standard Brazilian test procedure utilizing the recommended compression test machine according to Lepique (2008). The results demonstrated no statistically significant difference between the two methods.

3.3 Numerical discontinuum modeling of the Bliggspitze rock slide

We use the 2D mechanical modeling framework UDEC – Universal Distinct Element Code by Itasca Consulting Group (2019) – to analyze the mechanics triggering the first-time formation of the Bliggspitze rock slide. UDEC uses the distinct element method to represent the rock mass by defined discrete discontinuities, such as joints or faults and individual blocks resulting from the intersection of discontinuities. During simulation, those discontinuities (i.e., contact areas of two blocks) act as boundaries that allow sliding, toppling, or rotating of individual blocks. The blocks can be represented by a continuum (zoning of finite-difference element mesh) and are deformable according to assigned constitutive material models. We apply the Mohr–Coulomb slip criterion in our modeling scenarios to represent shearing along discontinuities. We assigned linear elastic (elastic, isotropic model) or elastoplastic (Mohr–Coulomb model) as constitutive material models to blocks representing rock mass or glacier ice, respectively. The geologic 2D model of Bliggspitze (for the location of the profile, see Fig. 1; the structural geology is shown in Fig. 3a) was used for the mechanical analysis.

3.3.1 Implications of the glaciers' thermal regime change on permafrost and hydrogeology

The Bliggspitze rock slope was almost entirely covered by the Northern Bliggferner Glacier before the first-time formation of the Bliggspitze rock slide. The Northern Bliggferner Glacier, which ranges in elevation from 2800 to 3200 ± 20 m a.s.l., excluding the ice apron above the bergschrund that reaches elevations of up to 3360 m a.s.l., spanned approximately 1 km in length in 2006 and can be characterized as a polythermal glacier of type D according to classification of Pettersson (2004). Cold ice is restricted to uppermost accumulation area, whereas low altitudes exhibit warm ice. These glacier types are common at high altitudes in the European Alps (Suter, 2002). Permafrost and hydrogeology are strongly affected by the basal regime of the overlying glacier. Inferred from observation of the evolution of the Northern Bliggferner Glacier, as shown in Sect. 4.1, we drafted a generic model coupling the interdependencies of glaciers' basal regime, permafrost, and hydrogeology. We define the border between a glacier's cold and warm base as the polythermal dividing line (PDL, Fig. 3b). At elevations below the PDL, the glacier has a warm base, meaning basal discharge is possible and meltwater can infiltrate into the bedrock where permafrost is absent. However, at elevations above the PDL, the glacier has a cold base, indicating the existence of permafrost and hindering surficial water from reaching bedrock. For simplicity, we assume that permafrost is bound to the elevation of the PDL. Especially in spring, when meltwater discharge reaches seasonal peaks, groundwater levels rise temporarily. We use the elevation of the PDL and slope topography as upper limits to model a free water table under peak discharge conditions. Similar to a shift in the equilibrium line altitude, we hypothesize that the PDL is also shifting to higher elevations under a warming climate. We investigate the mechanic response of the rock slope to permafrost degradation and peak groundwater level, with both simulated as a function of the elevation of the PDL, which was iteratively increased by $\Delta h_{\mathrm{PDL}} = +30$ m after each mechanical simulation (Fig. 3b).

3.3.2 Scenario analysis

We developed four individual scenarios, i.e., S1 to S4 (Fig. 3). In the first step, we evaluated the rock slope's predisposition to failure by testing the model with varying compositions of structural elements, such as fault zones, joints, foliation, and basal shear zone (scenario S1). As a result of scenario S1, we progress with a model of representative geometry to assess the mechanical effect of glacier unloading (S2), permafrost degradation (S3), and peak groundwater level (S4) as potential triggers for failure. Figure 3c summarizes the detailed parameterization of each scenario and the underlying assumptions. Subsequently, we describe each scenario in detail.

S1 – structural predisposition. In the first scenario, we assess which mapped structural features are relevant in controlling slope displacement. The given 2D cross-section aligns with the direction of kinematic movement. The distribution and direction of fault zones and the basal shear zone were adopted according to Zangerl et al. (2019). For the foliation and the existing four joint sets, we calculated the mean apparent dip and projected it into the cross-section. Joint sets of which the strike forms a sharp angle with the strike of the cross-section smaller than 60° were not considered, as

these structures were not mechanically relevant. The model geometries A to F distinguish themselves by containing a different degree of structural complexity. We assumed that before the formation of the rock slide in 2007, the rock slopes' factor of safety must have been slightly > 1, representing a situation where the driving forces are only marginally smaller than the resisting forces. By varying shear parameters, i.e., the pairs of joint friction angle and joint cohesion that were assigned to all discontinuities within each respective model geometry, we aimed to identify states of the rock slope that are close to failure. For scenario S1, the assigned rock mass properties were calculated using values obtained by the Geological Strength Index characterization (Hoek and Brown, 2019) and intact rock properties from laboratory experiments (Table S1 in the Supplement). These values were kept constant for all further simulations.

S2 – glacier unloading. We modeled the Northern Bliggferner Glacier as two elastoplastic blocks representing the upper and lower part (Fig. 2a). Mass loss of the glaciers was simulated by assigning different densities to the modeled glaciers. The material parameters of the elastoplastic blocks, as well as the shear parameter for the boundary between glacier and bedrock, were determined by sensitivity tests according to the following criteria. (i) To account for the ductile behavior of ice, the glacier should exert minimal resistance against deformation when interacting with the rock mass. (ii) While the glacier body does not deform under its weight, it should remain stable and not shear off the bedrock contact. Except for the density of glacier ice, the material parameters were kept constant throughout all stages (Fig. 3c). Based on the assumed original state, the density of the glaciers was doubled or halved or the glaciers themselves were removed before the start of cycling to demonstrate the effect of glacial buttressing or loss of toe support on slope stability.

S3 – permafrost degradation. We assume a uniform permafrost distribution above the mountain permafrost altitude (MPA) where frozen rock prevails. Permafrost is absent below the MPA, and the rock is unfrozen. In the case of Bliggspitze, the MPA is equal to the elevation of the PDL (Fig. 3b, $h_{\mathrm{MPA}} = h_{\mathrm{PDL}}$). We incorporated the effect of permafrost by assigning higher shear parameters to discontinuities within the frozen rock. In sub-scenario S3A, we run simulations with a surplus in friction angle of $\Delta\phi = +5^{\circ}$ for frozen in respect to unfrozen rock, while cohesion c remained unchanged. In sub-scenario S3B, we run simulations taking into account both the effect of ice-filled joints $\Delta\phi = +5^{\circ}$ and the effect of frozen rock bridges $\Delta c = +0.02$ MPa on shear strength of discontinuities within the frozen area.

S4 – peak groundwater level. Scenario S4 investigates the impact of temporary peak groundwater levels initiated by an excess supply of meltwater or rainfall. The elevation of PDL defines the horizontal boundary below which a free water table may exist within the rock mass (Fig. 3b, $h_{\mathrm{PDL}} = h_{\mathrm{wl}}$). The slope topography at elevations below the PDL defines the surface of the free water level, assuming fully saturated rock mass. In UDEC, hydrostatic pressure was exerted within all discontinuities below the water table throughout the full cycle time. According to the principle of effective stress, the total stress is diminished by the water pressure present at each specific location. Stress-related variation in joint aperture was ignored. Given the dense fracture network of the rock slope, which exhibits loosened blocks and joint spacings up to decameters at surfaces, water permeability is likely to remain unaffected by variations in joint aperture. The mechanical response of the model did not influence the hydrogeological situation. Hydrostatic pressure was applied only within discontinuities; blocks were assumed to be impermeable.

3.3.3 Model initialization and simulation workflow

Subsequently, we describe the initialization of the mechanical model. We refined the mechanical model according to topography and structural geological features, introducing them as discontinuities. The meshing of blocks was performed with a maximum edge length of 10 m. To enable the rotation of blocks and reduce overall execution time, the rounding length of corners was set to 0.5 m. The left, bottom, and suitable model boundaries were fixed with no-velocity conditions. The gravitational force was assigned to $9.81\,\mathrm{m\,s^{-2}}$. To account for the topographic effect on stress distribution, we initialized models with a vertical in situ stress ratio of $k = 0.5$ ($0.5\sigma_y = \sigma_x = \sigma_z$). For initializing a base model serving as a starting point for the simulation of each single scenario, we applied shear strength values of $\phi = 40^{\circ}$ and $c = 0.5$ MPa to discontinuities and bulk and shear moduli of $K = 37$ GPa and $G = 14$ GPa, respectively, to the blocks being modeled as linear elastic entities. The base model was then solved until equilibrium was reached, after which deformations were reset to zero. The calculated stress state of the base model represents the initial condition for the scenario simulations.

The procedure for analyzing individual scenarios based on the initialized and properly parameterized model is described below and illustrated in Fig. S1 of the Supplement. For each simulation, we ran 10 000 mechanical time step cycles and recorded 9 different histories at monitoring points within parts of the rock mass and the glacier that are expected to be either displaced or stable. We visually compared the displacement results of the overall model at the end of cycling and inspected the displacement as a function of the mechanical time step cycled for the selected monitoring points. If the displacement of the unstable parts within the rock mass approaches an equilibrium state by the end of cycling, meaning after initial settlement, the slope restabilized itself; we assumed the overall slope to be mechanically stable. We evaluated the slope stability by comparing the displacement value of a monitoring point at the end of cycling versus its value 1000 mechanical time steps before. We described the slope as

stable if the difference was smaller than 0.1 mm. In contrast, if it was unstable, we cycled 10 000 mechanical time steps to check whether the model restabilized itself with some delay or decided that total slope failure occurred due to the unstable model.

Changes in the cryosphere were simulated semi-dynamically by a stagewise model update. A stage represents a specific stadium of a glacier determined by the attributed load of the glacier in terms of mass m_{ice} (S2), or a specific elevation of the PDL (S3 and S4). In the case of scenario S1, a stage represents a specific pair of shear parameters assigned to all discontinuities in the model domain. According to the selected scenario, we upgraded the stage after the end of cycling, and the decision on slope stability was made to compute for the next stage. With this approach, we iteratively simulated the mechanical response to observed shifts in cryosphere, such as a gradual increase in PDL to higher elevations.

4 Results

4.1 Pre-failure analysis of the Bliggspitze rock slide

4.1.1 Evolution of the Northern Bliggferner Glacier

In the decades preceding the formation of the Bliggspitze rock slide, the Northern Bliggferner Glacier exhibited fluctuations in the rate of elevation change for the upper part, which appeared to neutralize the local effects of ice loss and gain (Fig. 4a). The lower part of the glacier exhibits a distinct loss in the range between 0 and $-1.3\,\mathrm{m\,yr^{-1}}$. In the period 2000–2012, covering the event of the rock slide, the upper part experienced a pronounced loss due to the slope deformation, and the lower part gains in elevation due to the deposits of the destabilized material from the Bliggspitze rock slide and other, smaller rock and ice avalanches during the respective observation period. The post-failure period indicates a process of glacier ice degradation in the upper part, while a gain in elevation is observed in the less steep lower part. The positive rate of elevation change observed at the glacier front in the post-failure period is attributed to two main factors. Firstly, the deposits resulting from the ongoing activity of rock–ice falls and avalanches and debris flows, which partly cover the glacier ice, contribute to the gain in elevation. Secondly, the dynamics of ice flow transport glacier ice from the steeper to the shallower slope, where the conservation of ice is extended by the insulating effect of debris cover despite the relatively shallow altitudes. The glacier thickness models indicate a loss of $30 \pm 5\,\mathrm{m}$ in the lower part of the glacier between 1970 and 2003 (Fig. 4b). In contrast, the upper part exhibited a less pronounced loss, with values generally below 10 m.

A comparison of historic orthophotography taken in the years of 1969 and 2003 from the upper section of the glacier where the head scarp is located (see Fig. 1) shows the evolution of the glacier using several features, such as the opening of new crevasses, loss of ice aprons, loss of small glacier branch at side, and drawdown of ice in proximity to the randkluft (Fig. 5). A cone-like depression structure becomes evident in the right center of the 2003 orthophoto. The scarcity of snow cover and streamlines in the right part of both orthophotos is attributed to avalanches favored by the steep rock faces above the glacier. In 1969, the bergschrund is clearly imprinted as a prominent transverse crevasse forming under extensive extensional stress (Fig. 5a, area 1). Further upglacier in an arch shape just below and following the ridge, a narrower fracture band is visible. In the west, this linear fracture turns into a sequence of lateral crevasses. A total of 34 years later (Fig. 5b), after the glacier surface steepened and lowered by about 10 m in the upper reaches, the crevasse pattern changed. The former bergschrund is clearly visible but snow covered. Its location hardly changed. Moreover, a new gaping fracture has opened just above the old bergschrund. The fracture arch further upstream is no longer a single line feature but disintegrated into many shorter extensional fractures, with some forming a crevasse sequence. All of the new features are associated with increasing extensional stress.

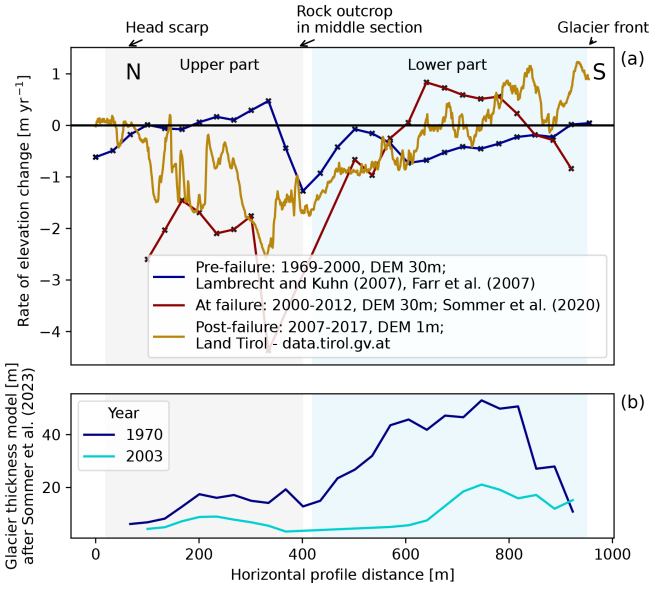

Figure 4. **(a)** Rate of annual elevation change for given periods calculated along the longitudinal N–S cross-section of the Northern Bliggferner Glacier, oriented in the direction of ice flow. **(b)** Glacier thickness model according to Sommer et al. (2023) showing the pronounced loss in the lower part between 1969 and 2003. The trace of the cross-section is displayed in Figs. 1 and S3. The segmentation of the Northern Bliggferner Glacier into an upper and lower part is shown in Fig. 2a and 12.

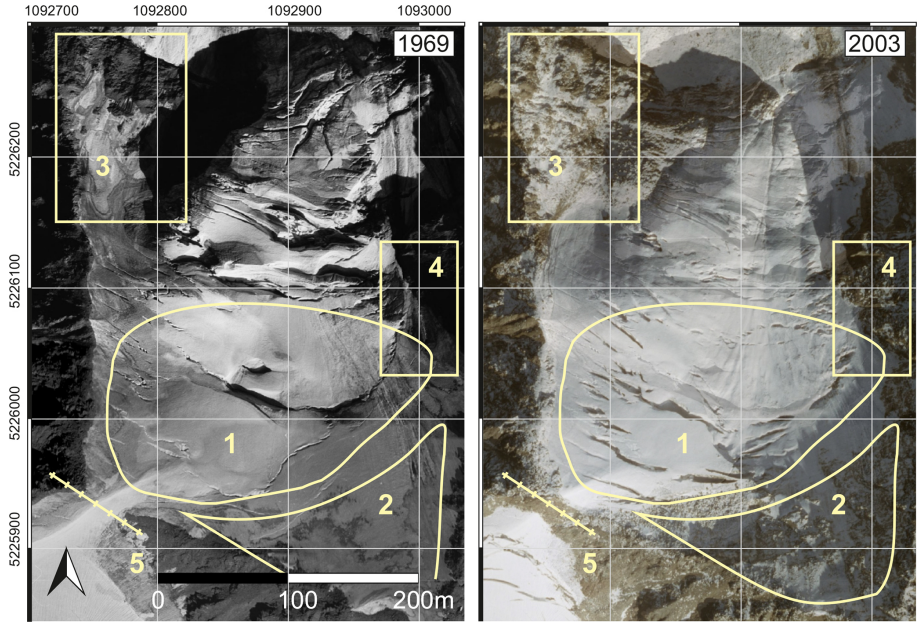

Figure 5. Evolution of the upper part of the Northern Bliggferner Glacier by visual inspection of aerial photographs of the years 1969 and 2003 (data provided by Land Tirol – https://www.tirol.gv.at/data/). Description of the features that changed during the 34-year interval: (1) opening of new crevasses, (2) loss of ice apron above the bergschrund, (3) loss of a small branch of the glacier, (4) decrease in glacier thickness visible through exposure to new rock exceeding several meters, (5) loss of conjunction between Northern Bliggferner Glacier and Southern Bliggferner Glacier. For an overview of the location, refer to Fig. 1.

4.1.2 Indication of permafrost in the area of the failure volume

The presence of permafrost in the area of the head scarp created by the rock slide is evident by the observation of ice-filled fractures and the ice aprons above the bergschrund (Fig. 2d). Permafrost conditions are further characterized by the analysis of ground surface temperature (GST), electrical resistivity tomography (ERT) conducted on 12 August 2009, and electrical conductivity of mapped springs in 2011/2012 (for the position, see Fig. 1).

From September 2013 to August 2016, 22 ground surface temperature (GST) loggers were placed in the area of the head scarp within niches in the blocky terrain close to the topographic surface. All loggers showed mean temperatures of −4 to −1 °C overall (Fig. 1). The upper and lower percentile of every GST record falls within a range of 0 to −0.5 °C and −3 °C to −7.5 °C, respectively (Fig. S2). Considering each hydrological year and GST record, the average number of annual freezing degree days (mean GST below 0 °C) is 322. Most logger recordings showed a dependence of GST and incoming solar radiation: the lower the potential incoming solar radiation, the colder the mean annual temperatures (Fig. 1). The GSTs varied significantly in zero-curtain duration and winter air temperature signal penetration. From September 2014 to August 2015, extended zero-curtain periods were evident, marked by daily standard deviations below 0.001 °C. The preceding and following years showed fewer zero-curtain days and indicated less buffering of air temperature signals in autumn, winter, and spring. Most GST records suggest snow-free conditions only in August and September, with daily standard deviations above 0.5 °C and GST closely following air temperature. Figure 6 exemplifies the spread of heterogeneous records by drawing temperature for the coldest recorded mean, a mid-temperature mean, and the warmest recorded mean of the GST loggers. The record of logger S11 follows the trend of air temperature (AT) in a pronounced way and indicates snow-free windows or little snow cover throughout the year. In contrast, the location of the logger S12 is covered with snow for a minimum of 10 months a year. Nearly isothermal conditions are kept throughout winter and spring, with only light response to AT changing. Apart from S12, all other GST loggers resulted in maximum daily temperatures below −3 °C within the months of February and March, suggesting probable permafrost conditions according to Haeberli (1973).

We carried out ERT on 12 August 2009, 2 years after the first-time formation of the rock slide. The transect was located in the upper part of the fragmented rock mass that was covered with glacier ice before displacement. The transect starts at the contact between the fragmented rock mass and the basal shear zone following the direction of mass movement (see Fig. 1). The inversion result of the electrical resistivity tomography (ERT) indicates the following subsurface situation (Fig. 7): at shallow depths, high resistivities above 10 000 Ω m are documented, most likely represent-

ing the fragmented, blocky rock mass with a high amount of air-filled voids that were clearly visible at the surface. The high density of contour intervals at profile meters 45 to 75 illustrates a decrease in resistivity by approaching higher depths. The low resistivities below 1000 Ω m indicate water-saturated compartments within the rock mass. Compartments in the mid-range of plotted resistivity values most likely represent a combination of voids within the rock mass and partially saturated areas. No clear evidence for frozen subsurface conditions could be found due to resistivities generally below 20 000 Ω m.

We categorized the 32 springs according to the geomorphological forms in their vicinity and assigned the most probable source of the water origin (Fig. 8). A pronounced cluster of springs with high conductivity ($> 150\,\mathrm{mS\,cm^{-1}}$) was observed, especially in proximity to the slopes surrounding the Northern Bliggferner Glacier (see Fig. 1, which depicts the location of 18 out of 32 springs in the map). Additionally, two springs with high conductivity were attributed to rock glaciers, and one spring is directly linked to glacial discharge near the tongue of Northern Bliggferner Glacier. All other springs had electrical conductivity values below $150\,\mu\mathrm{S\,cm^{-1}}$. These included springs at different slopes at a greater distance to the head scarp, at moraines, at rock glaciers, and springs related to corridors of glacier discharge in a more distal area, as well as springs attributed to the catchment area of other glaciers.

4.1.3 Chronology and description of the formation of the rock slide

A comparison of the climate during the period before the first-time formation of the rock slide with the long-term climatic conditions between 1780 and 2007 revealed that the period from January to June in 2007, before the rock slide in 2007, was the warmest in a 227-year climate record (Fig. 9). In 2007, the mean temperatures of the individual months January to March lay above the 75th percentile, April was the warmest month of the entire record, and May and June reached temperatures above the 75th percentile. Compared to the hot summer in 2003, winter and early spring also saw months with comparatively high average temperatures in 2007 (Fig. 9). Consequently, the period preceding the rock slide was characterized by elevated air temperatures for several months.

Before the formation the rock slide on 29 June 2007, several debris flows and rock falls had been noticed in the previous years. We confirmed this by examining photographs of the northwest-facing steep slope directly connected to the Northern Bliggferner Glacier. The activity of debris flows is evident by the erosion creating incised gullies (see Fig. 1, change detection) and enlargement of talus in comparison to the state in 2003 (Fig. 2a, b). In the narrow time window days before the rock slide, optical signs such as dislocation cracks in fresh snow, low-magnitude rock and ice falls, and water leakages in slopes and at rock outcrops were evident.

The rock slide was triggered at the end of a cold front that arrived 4 d earlier. The arrival of the cold front is marked by a daily precipitation sum of 20 mm, a drop in air temperature below 0 °C, and a distinct drop in water temperatures of glacier discharge (Fig. 10 a, b). The records from the Vernagtbach meteo station, 8 km from the Bliggspitze site, served as a proxy for glacier melt and snowmelt. From 17 to 26 June, discharge steadily increased, with electrical conductivity inversely related to this rise (Fig. 10b). The 25 June 2007 precipitation event is evident in the discharge record, with a tailing effect seen in the days following. The formation of the rock slide happened at a time that aligns with the daily peak in measured water temperature (Fig. 10b) at 11:23 LT (local time), which was recorded on video – a time sequence of images showing the evolving rock–ice avalanche that resulted from the rock slide can be found in Fig. 1 in Pudasaini and Krautblatter (2014).

The photograph in Fig. 2d) was captured hours after first-time formation of the rock slide. The rock slide led to the fragmentation of the glacier ice and the exposure of previously ice-sealed bedrock (Fig. 2e). In the days after the event, eye-catching springs within steeper slope sections close to the glacier were present. Orthophotographs recorded in the time interval between 2007–2009 and 2009–2012 indicate ongoing debris flow activity by streamlines and wet areas at the surfaces of the west-facing slopes below Northern Bliggferner Glacier (Fig. S3).

4.2 Laboratory experiments of anisotropic rock under frozen and unfrozen conditions

In addition to existing rock mechanical data related to permafrost dynamics, we investigated tensile strength as the most unknown and most sensitive parameter to thermal changes. We conducted destructive pseudo-Brazilian tests (BZT) on paragneissic rock samples to gain rock mechanical parameters simulating unfrozen conditions and frozen conditions. The difference between the two conditions is statistically significant (p value and t statistic of unpaired T test: 5×10^{-9}, 7.10 ($n = 52$)). We found that tensile σ_t is higher for frozen than unfrozen states (Fig. 11). The mean value for $\sigma_{t,\mathrm{frozen}}$ is 10.78 MPa, and for $\sigma_{t,\mathrm{unfrozen}}$ it is 6.50 MPa. The mean relative decrease in σ_t, transitioning from the frozen to the unfrozen state, is −40 %. Observing tensile strength as a function of the orientation of the foliation, a decrease in tensile strength transitioning from favorable to unfavorable orientation regarding force direction becomes apparent. Comparing one extreme case $\angle_{\boldsymbol{F}_t/\mathrm{fo}} = 0°$, with the other extreme $\angle_{\boldsymbol{F}_t/\mathrm{fo}} = 90°$, a strength loss depending on the foliation orientation is evident. In extreme cases, the loss is more pronounced for frozen than for unfrozen states. However, cases representing the arbitrary orientation of foliation, such as those tested with $\angle_{\boldsymbol{F}_t/\mathrm{fo}} = 45$ or 70°, do not indicate this

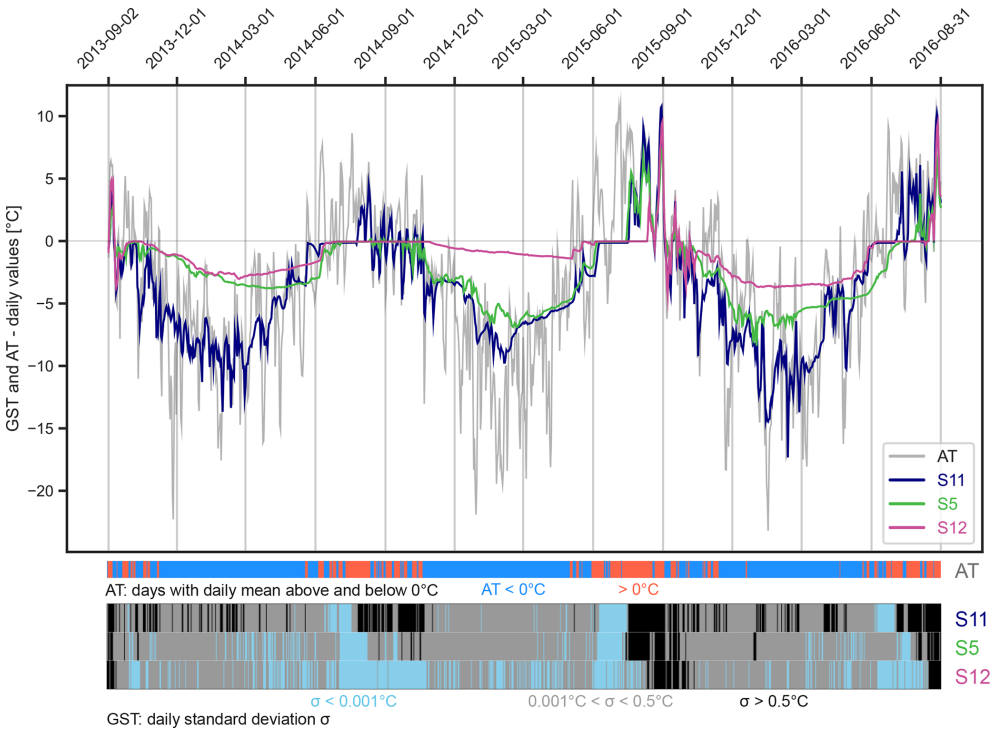

Figure 6. Ground surface temperature plotted for three distinct logger recordings showing strong heterogeneity in permafrost-favorable conditions. Refer to Fig. 1 for logger positions. The data were reanalyzed from data of Zangerl et al. (2019). A proxy for air temperature (AT) is modeled at the head scarp at an altitude of 3200 m a.s.l. The difference in mean daily AT of two nearby meteo stations within a radius of 8 km (Pitztal Glacier at 2863.9 m a.s.l. and Brunnenkogel at 3437 m a.s.l.) was calculated daily and projected to the corresponding altitude using a linear model.

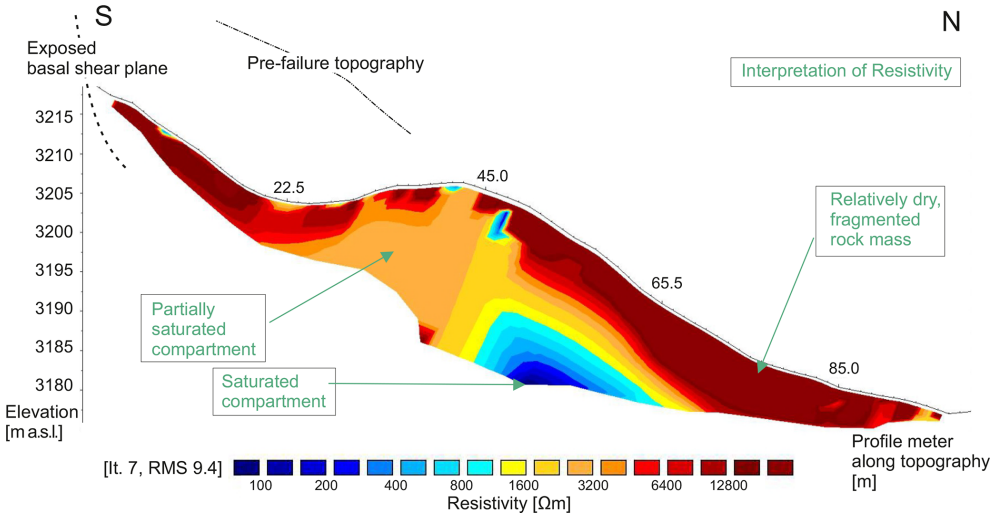

Figure 7. Inversion result of electrical resistivity tomography conducted on the failed rock mass near the head scarp. The green-colored information in boxes illustrates the most probable interpretation of subsurface areas based on resistivity values as suggested in studies with similar lithology by Krautblatter and Hauck (2007); Keuschnig et al. (2017); Offer et al. (2024). For the location of the profile, see Fig. 1.

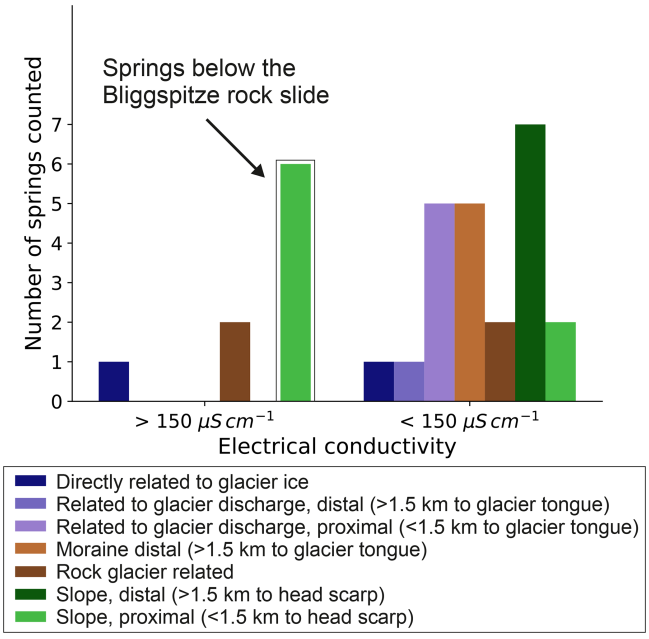

Figure 8. Categorical plot of 32 classified spring types concerning high or low measured electrical conductivity in the area surrounding the study site. Six springs with high conductivity are located at the west-facing slope directly below the Bliggspitze rock slope. The reanalyzed data were measured in the summer of 2011/2012 (Dejean de la Bâtie, 2016).

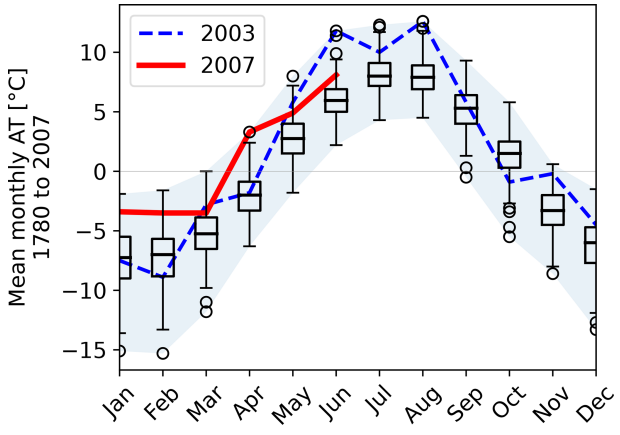

Figure 9. Climatic conditions at the study site over a 227-year period (1780–2007), represented by monthly air temperatures (AT) using boxplots. The boxplots illustrate the distribution of temperatures for each month, highlighting median values, interquartile ranges (IQRs), whiskers (marked by $1.5 \cdot \mathrm{IQR}$), and outliers. The shaded area illustrates the range of historic air temperatures for the respective months. The red line illustrates the monthly temperature in 2007 prior to the formation of the rock slide (HISTALP dataset of corresponding 5 min grid cell, GeoSphere Austria (2023)).

trend. The surplus of tensile strength by freezing is more pronounced for favorable orientation $\angle_{\boldsymbol{F}_t/\mathrm{fo}} = 0°$ than for unfavorable orientation $\angle_{\boldsymbol{F}_t/\mathrm{fo}} = 90°$. In general, the transition from an unfrozen to a frozen state is more pronounced in tensile strength than the transition from an unfavorable to a favorable foliation orientation.

4.3 Numerical discontinuum modeling of the Bliggspitze rock slide

The mechanical modeling study was designed using multiple scenarios (S1 to S4; see Fig. 3). In the initial scenario, we investigated the effect of structural predisposition, as defined by the geology and the geometry of the rock slope (S1). In the second scenario, based on the results of the previous scenario S1, we analyzed the impact of cryospheric forcing on slope stability for three individual scenarios: S2 (glacier unloading), S3 (loss of permafrost), and S4 (peak groundwater level).

The concept of the polythermal dividing line (PDL) results from the investigations of the cryosphere, presented in Sect. 4.1. It includes the consideration of the interplay between the glaciers' thermal regime, permafrost, and hydrogeology. The deviation of the concept is explained in Sect. 3 (see also Fig. 3). The concept is applied in order to model the mechanical response of the rock slope as the glacier transitions from a cold to a warm glacier ice regime while impacting permafrost distribution (S3) and hydrogeologic conditions (S4). The results of the simulations of individual scenarios are presented first, followed by the results of the combined scenario simulations.

S1 – Structural predisposition. We examined six model geometries (A–F) with varying levels of detail of structural features to assess the structural control on the rock slope (Table 3). The degree of detail builds upon the previous level: fault zones only (A), plus joints (B), and plus foliation (C). For the model versions D to F we included the basal shear zone and repeated the previous sequence. As an example, the model geometry of E, including fault zones, joint sets, the basal shear zone, and the location of monitoring points that are used to evaluate the displacement of the rock slope, are shown in Fig. 12a. All tested model geometries and model states at the end of cycling can be visually compared in Fig. S4. Subsequently, the results of the sensitivity study on structural features characterizing the rock slope are presented.

For all tested geometries, the inclined fault zone delineating the head scarp (Fig. 3a; see fault zone "fi") showed the highest shear displacement at states close to failure. For the models with geometry A to C, only stable states were reached. The geometry of intersected rock mass and the behavior of the linear elastic block models restrict the deformability of the rock mass, even at unrealistically low shear strength values. In the case of geometry A to C, discontinuities do not dip out of the slope and the slope restabilized itself after initial displacement. Along vertical fault zones, upward-facing scarps were created at various pairs of shear properties within the tested range ($\phi = 40$ to $25, c =$

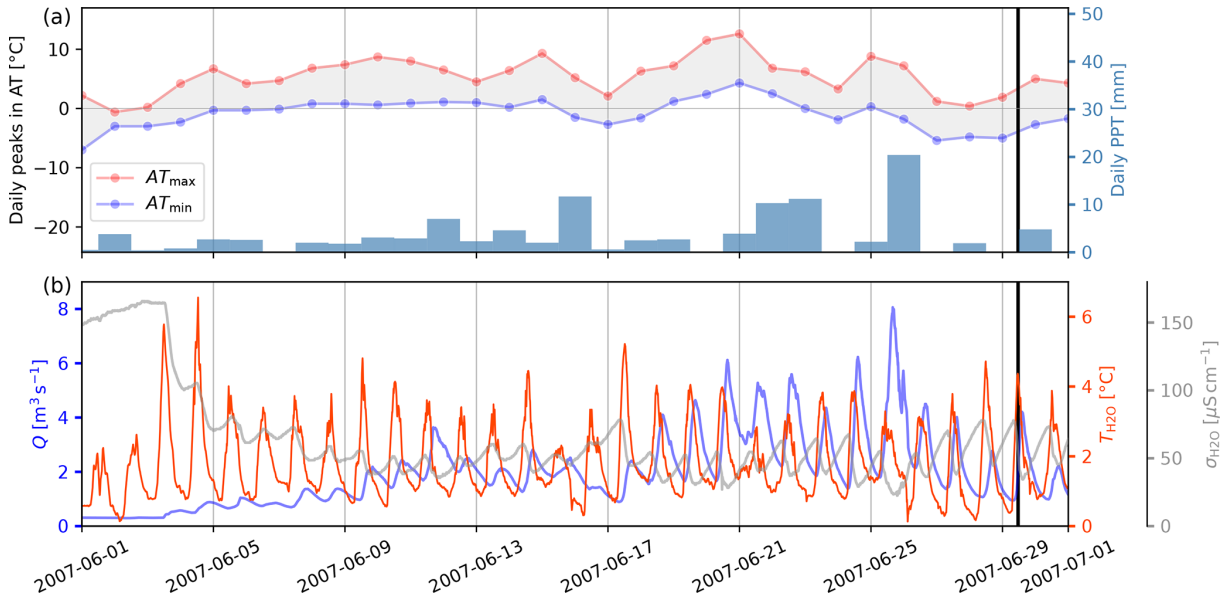

Figure 10. **(a)** Weather conditions and **(b)** meltwater discharge in the weeks before the rock slide occurring on 29 June 2007 at 11:23 LT. The vertical black line marks the timing of failure. **(a)** Daily peak air temperatures (AT) and total precipitation (PPT) for the grid cell of Bliggspitze field site (SPARTACUS dataset for the corresponding 1 × 1 km grid cell, GeoSphere Austria (2023)). **(b)** Hydrological record of the Vernagt basin: water discharge (Q), water temperature (T_{H_2O}), and electrical conductivity (σ_{H_2O}) measured at 10 min intervals. The location of the hydrological station is in the Oetztal at 2640 m a.s.l., 8 km air distance from the Bliggspitze field site (dataset published by Escher-Vetter et al., 2014).

Table 3. Set of model geometries used in scenario S1 for testing the structural control of the rock slope. The corresponding results are given for shear parameters of discontinuities of $\phi = 30°$ and $c = 0.1$ MPa and for the model state after cycling 10 000 mechanical time steps. Structural features marked with an asterisk are integrated in the corresponding model geometry.

Geometry	Fault zones	Joints	Foliation	Basal shear zone	State at end of cycling	Max. displacement [m] within the model domain
A	*				stable	0.123
B	*	*			stable	0.099
C	*	*	*		stable	0.116
C.fo	*	*	*		stable	0.095
D	*			*	stable	0.130
E	*	*		*	stable	0.122
F	*	*	*	*	stable	0.126
F.fo	*	*	*	*	stable	0.105

The inclusion of "fo" indicates that discontinuities representing foliation structures are assigned higher values of friction angle: $\Delta\phi = +3°$.

0.5 to 0.01 MPa). The offset of the resulting scarps was limited to a size of less than a centimeter. For geometry C, we included the foliation incorporated as a set of discontinuities and assigned (a) the same shear strength value to all discontinuities or (b) assigned slightly higher values to the foliation than for other discontinuities ($\Delta\phi = +3°$). For the case of (a), overall shear displacement was accumulated over many neighboring foliation structures in the center of the slope, while in the case of (b) shearing along foliation structures was hardly activated. By integrating the basal shear zone with geometry D, slope displacement could now propagate until complete slope failure occurred. Comparing results of geometry D with geometry F, we observed larger total displacement within the full model domain when the model contained fewer structural features. A highly intersected rock mass containing more individual blocks due to a more detailed model geometry was found to be more susceptible to the interlocking of individual rotating blocks and could hinder further displacement. Figure 13 shows the result of sensitivity analysis for the different pairs of friction angle and cohesion for geometry E (fault zones, joints, and basal shear zone) by the history of the monitoring point Rm_x, which is located at the center of gravity of the displaced rock mass. Stable conditions of the rock slope can be achieved with either a rela-

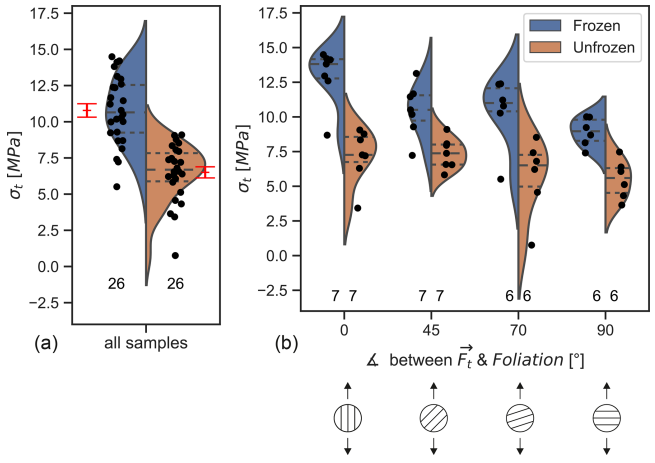

Figure 11. Tensile strength as a function of **(a)** frozen and unfrozen states and **(b)** the state and foliation of the paragneissic rock samples. Panel **(a)** shows the full pool of samples tested for frozen and unfrozen states. The red error bars indicate $\overline{x}$ and SD for the respective state. **(b)** Categorization of the samples according to tests conducted at different angles between loading force direction $\boldsymbol{F}_t$ and foliation orientation; see the sketches at the bottom of the figure. The number of samples tested is given at the bottom of the graphs, ranging from 6 to 26.

tively high friction angle and low cohesion or vice versa. All models with different geometries but the same shear properties of joints reached a stable state at the end of cycling. Due to high similarities at mechanic behavior and resulting maximum displacement, which varies in a range of 0.035 m, we decided to proceed with geometry E, representing the pre-failure state of the rock slope (Fig. 12). Unless otherwise specified, we fixed shear parameters of discontinuities to $\phi = 30°$, $c = 0.1$ MPa for modeling subsequent scenarios.

S2 – Glacier unloading. We assigned varying densities to the geometrical model of the lower and upper part of the Northern Bliggferner Glacier (Fig. 12a) and tested nine different stages accounting for arbitrary glacier thickness. Figure 14 displays the maximum displacement of the monitoring point Rm_x after the calculation of 10 000 mechanical time steps according to different assumptions made about the glacier mass. All tested stages resulted in stable slope conditions with x displacements varying in a range from 0.04 to 0.08 m. We simulated gradual glacier mass loss by the comparison of stages with doubled ice density (7), with the assumed initial density (2), with the halved-density glacier model (3), and with glacier-free conditions (8). The results showed ambiguous behavior. Higher normal load applied by glacier ice results in higher x displacement of 0.045 m (7), whereas a loss towards the assumed original stage (2) results in slightly lower x displacement of 0.04 m. A further loss of glacier ice (3) does not indicate a distinct effect on x displacement, whereas the glacier-free stage (8) results in the highest displacement of the four compared stages: 0.06 m. Stage 9 simulates the total loss of the lower part of the glacier, whereas the upper part remained unchanged, resulting in the highest of the observed x displacements of 0.08 m.

S3 – Permafrost distribution. According to the elevation of the polythermal dividing line (PDL) of the Northern Bliggferner Glacier covering the rock slope, we divided the model into an upper frozen and lower unfrozen part (Fig. 12b) and assigned a higher shear strength to frozen states of discontinuities (for sub-scenario S3A: $\Delta\phi = +5°$, $\Delta c = 0$ MPa; for sub-scenario S3B: $\Delta\phi = +5°$, $\Delta c = +0.02$ MPa) than for unfrozen states. Through an iterative rise in the PDL, the history of monitoring point Rm_x indicates displacements in the range of centimeters for low PDLs (Fig. 15). Simulating the retreat of permafrost with increasing PDL, the maximum x displacement approached the magnitude of a decimeter, while the overall model remained stable for both S3A and S3B. Up to a specific elevation of PDL, a clear but constant difference in x displacements was notable between S3A and S3B within the same stages. However, when the PDL reached an elevation higher than 3100 m a.s.l., meaning that the observed grid point Rm_x located at 3080 m a.s.l. is now in the unfrozen area, the difference was equalized.

S4 – Peak groundwater level. Peak groundwater levels result from peak meltwater discharge or peak precipitation events. The temporary rise in the water table resulting from the event is delineated by the PDL and slope topography (Fig. 12b and c). Water pressure is applied only within discontinuities according to the vertical offset to the defined water table. Simulating the rise in peak groundwater level as a consequence of gradual increasing PDL, we found that no stage reached a stable state due to initiated continuous shearing along the basal shear zone (Fig. 15). When the groundwater level, defined by the elevation of the PDL, exceeds the height of the outcrop of the basal shear zone, irreversible displacement is initiated, and the area of the rock mass above the basal shear zone propagates downwards. Total slope failure occurs already at simulated low elevations of PDL due to the loss of the rock buttress at the toe. The exerted hydrostatic water pressure pushed out single blocks at the toe of the rock slope and accelerated the mass above the basal shear zone that reached irreversible displacement (Fig. S5).

Remodeling initial rock slope state. As a consequence of the susceptibility of the slope to exerted hydrostatic pressure, we remodeled all scenarios with higher shear parameters of discontinuities ($\phi = 40°$, $c = 0.3$ MPa). These strength properties were determined by sensitivity analysis of scenario S4 under a fixed peak groundwater level at PDL of 3050 m a.s.l., representing the least stable state prior to a further rise in water level to a PDL of 3080 m a.s.l., which would result in total slope failure (for results, see Figs. 15 and 14, marked with opaque dots). Our simulation results showed a limited impact of glacier unloading and permafrost degradation on slope displacement. While all conducted simulations resulted in stable states at the end of cycling – displacements were

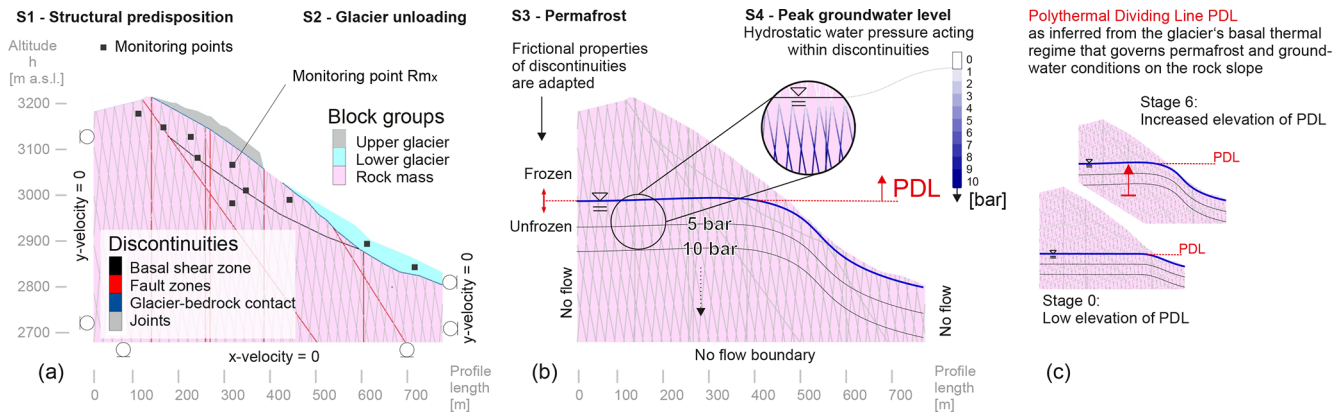

Figure 12. Implementation of model scenarios in UDEC. **(a)** The geometry of model E shows the internal structural features, the dimension and shape of the glaciers covering the rock slope, and the location of monitoring points used to control displacement history while cycling. **(b)** The polythermal dividing line (PDL) is shown for an arbitrary elevation to indicate its effects on permafrost and peak groundwater level (S3, S4). **(c)** Each stage in scenario S3 and S4 represents a certain elevation of PDL. With increasing stages, the elevation of PDL was increased. Note that the glaciers in **(a)** were not included in simulations of scenarios S1, S3, and S4.

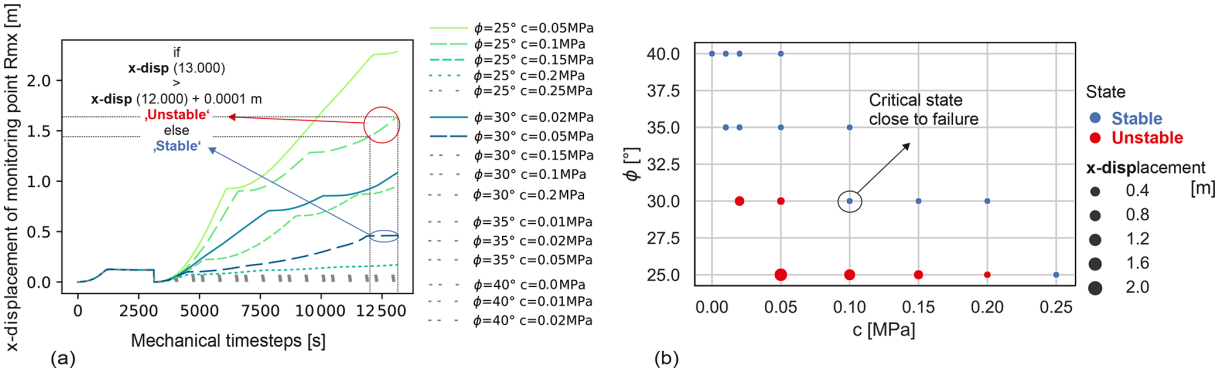

Figure 13. Sensitivity study of shear parameters, attributed to discontinuities in scenario S1 with geometry E, by analyzing the mechanic response by the history of monitoring point Rm_x. **(a)** Relationship between mechanical time steps versus x displacement of the observed grid point for given pairs of shear parameters. The given equation checks whether the model reaches equilibrium state at the end of cycling. The first 3000 mechanical time steps show the cycling of the initialized model until reaching equilibrium. **(b)** Maximum x displacement of Rm_x and model states plotted for specified pairs of shear parameters at the end of cycling.

generally below 10^{-1} and 10^{-3} m, respectively, for the case of the modeled pre-failure state and the remodeled state. Simulations results of scenario S3A and S3B, given the shear parameters according to the remodeled state, display marginal x displacements below 10^{-5} m, which were not considered to be within a relevant range and therefore ignored in the plot of Fig. 15. In contrast, applied water pressure within discontinuities, as simulated in scenario S4, led to total slope failure at the modeled pre-failure state when applied at the lowest parts of the basal shear zone only (displacements > 1 m). At the remodeled state in S4, slope displacement increased continuously from 10^{-3} to 10^{-1} m, concomitant with a rise in the groundwater table according to the PDL. The rock slope reached stable states at the end of cycling for elevations of PDL below 3050 m a.s.l. Total slope failure with x displacements > 1 m occurred at elevations of the PDL above 3050 m a.s.l., as defined by the back calculation of shear parameters for discontinuities (i.e., remodeled state; Fig. 15).

5 Discussion and limitations

5.1 Interactions between the glacier basal regime, hydrogeology, and permafrost

For a long time, glacier research in the Alps and permafrost research in the Arctic lowlands were treated separately (Haeberli, 2005). The strong interactions between them and their relevance for geomorphological landscape evolution have been highlighted by Etzelmüller and Hagen (2005) conceptualizing thermal glacier regimes related to mountain permafrost. Among one of several documented, $> 10^6$ m^3 rock–ice avalanches, the Mount Steller rock–ice avalanche (Alaska, 2005, release volume of $5\,(\pm 1) \times 10^7$ m^3) exempli-

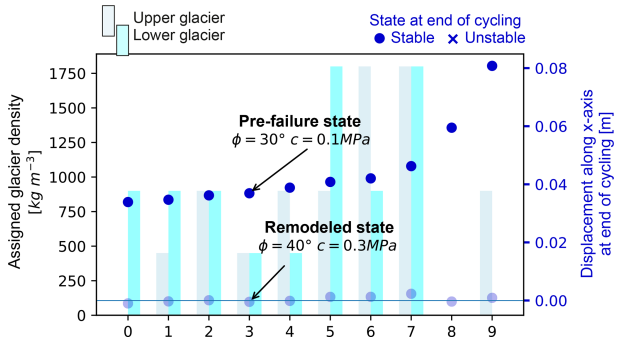

Figure 14. Scenario S2 simulates the effect of varying glacier mass on slope stability across nine specified stages. Results are illustrated for the end of cycling of 10 000 mechanical time steps. Geometries of the upper and lower part of Bliggferner are illustrated in Fig. 12a. The effect of mass unloading is simulated by the variation of assigned densities to the upper and lower parts of the Northern Bliggferner Glacier (see Fig. 3). Stage 2 displays the representative initial model with an approximate thickness of 30–40 m for the lower glacier and 20–30 m for the upper glacier with an attributed ice density of 917 kg m^{-3}. For example, stage 4 simulates a faster glacier mass loss at the lower part, whereas the upper part remains constant.

fies how steep mountain glaciers in cold permafrost conditions induce complex thermal anomalies, possibly increasing temperatures close to phase equilibrium at the glacier–bedrock interface, which was hypothesized to have triggered the detachment by warming permafrost and meltwater infiltration at the base of the glacier (Huggel et al., 2008). However, due to the remote locations and restricted accessibility of detachment zones of glacier-permafrost-related rock slope failures, datasets and observations are scarce and typically challenging to obtain (Haeberli, 2005; Huggel et al., 2008; Shugar et al., 2021; Geertsema et al., 2022). From a glaciological perspective, glacier instabilities of type 2 are triggered by the transition of steep and cold hanging glaciers into temperate regimes according to Faillettaz et al. (2015). Therefore, thermal modeling of the spatial and temporal evolution of the glacier bed temperature was emphasized in a first approach by Gilbert et al. (2015), who could clearly demonstrate a rise in the 0 °C isotherm at the glacier–bedrock interface to higher elevations over multiple decades. This study delves below the glacier–bedrock interface, analyzing glacier–permafrost interactions and their consequences on rock slope stability.

Results of the numerical modeling study suggest a distinct impact of fluctuating groundwater levels on the stability of the Bliggspitze rock slope. By employing the concept of a gradual rise in the cold–warm dividing line at the base of a polythermal glacier (PDL), high amounts of available water in spring and summer may reach bedrock surfaces that were previously sealed with cold glacier ice. The water then either discharges at the glacier base or infiltrates into the subsurface, resulting in a temporary rise in hydrostatic pressure within the fracture network. The Bliggspitze rock slide is likely to be prepared by transient hydrostatic pressures, as shown by the simplified model scenarios, yet the processes behind this are more complex and discussed subsequently by utilizing Fig. 16. Thinning of glacier ice under warming climate and reduced magnitude and/or time of cold winter temperatures penetrating the glacier ice indicates that the polythermal Northern Bliggferner Glacier is shifting towards a temperate regime. Conversely, glacier thinning under stagnant or cooling climate could also lead to the creation of extended cold ice compartments according to Irvine-Fynn et al. (2011), which is not the case for the Northern Bliggferner Glacier as (a) long-term trends in air temperature, (b) the accelerated loss of glacier ice visible at the lower part and the upper part in conjunction to the Southern Bliggferner Glacier between 1969 and 2003, (c) debris flows originating from the rock slope below the glacier that reflect high water availability as observed in the years and days before the first-time formation of the rock slide, and (d) active-layer deepening inferred from the high mineralization of springs indicate the shift towards a temperate regime. Although the altitude of the 0 °C isotherm of air temperature continuously increased since 1900, the full extent of the Northern Bliggferner Glacier remained considerably above the 0 °C isotherm (HISTALP dataset, Chimani et al., 2013). Thus, diffusive heat flow alone cannot describe the observed warming of the glacier, and advective heat transport must be considered a relevant process for warming glacier ice. Considering the rather cold climate, the aspect and slope of the terrain, and the stagnant glacier front between 1969 and 2006 (Fischer et al., 2015), the movement of the glacier must be marginal. Ground surface temperatures conducted in the years after the failure generally reveal permafrost-favorable conditions at the elevation of the head scarp. In contrast, the distinct loss of ice aprons above the Bergschrund of the Northern Bliggferner Glacier failure visibly demonstrates permafrost degradation in the decades before the failure.

In our generic model, we assumed (i) the existence of a single polythermal dividing line(PDL) at the bedrock–glacier contact point, (ii) that the mountain permafrost altitude (MPA) is bound to the elevation of the PDL that is gradually rising under a warming climate, and (iii) that the area below the PDL is unfrozen and discontinuities below the water table, which aligns with PDL and slope topography, are fully saturated. These idealistic perspectives are discussed below.

Firstly, the existence of cold basal glacier ice is dependent on the altitude and might also be distributed discontinuously, especially in complex topographic terrain and heterogeneous flow velocities (Cuffey and Paterson, 2010). We differentiate between warm and cold basal ice using temperature and basal discharge, which is only possible under warm ice at the base. In the case of the Northern Bliggferner Glacier, we

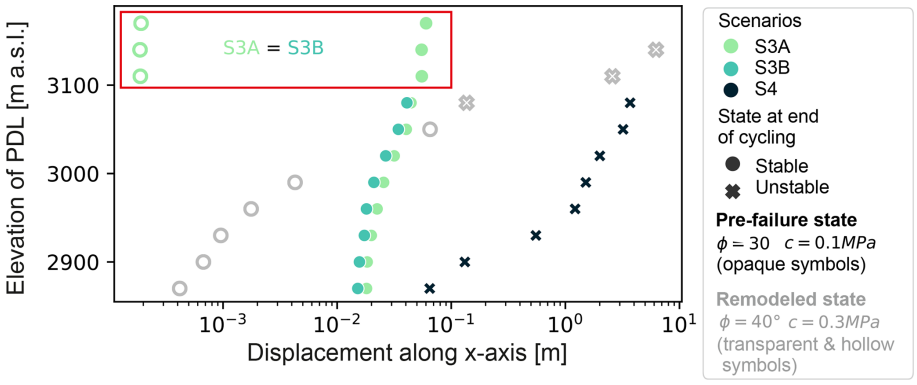

Figure 15. Semi-log plot of x displacement of monitoring point Rm_x after 10 000 mechanical time steps for scenarios S3 and S4 plotted against the elevation of the polythermal dividing line (PDL). The model geometry is according to S1E (see Fig. 12), and parameters are assigned according to Fig. 3. Results are displayed for shear parameters of discontinuities given in the lower-right part of the graph. The values represented within the orange box demonstrate that, for the specified elevation of the PDL, there is no discernible difference in x displacement between scenario S3A and S3B for both assumed original conditions of discontinuities, i.e., the pre-failure state and the remodeled state.

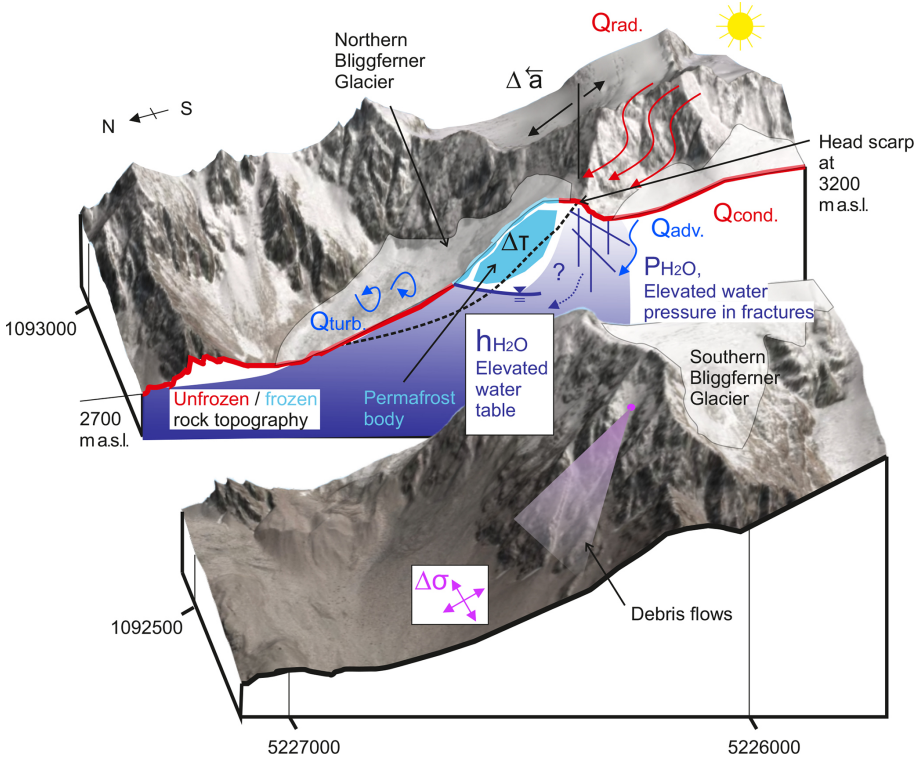

Figure 16. Holistic view on the manifold processes leading to the Bliggspitze rock slope failure. For discussion of individual concepts, refer to the text (Sect. 5.1). Various heat transport mechanisms such as $Q_{\mathrm{rad.}}$ (radiative heat), $Q_{\mathrm{cond.}}$ (conductive heat), $Q_{\mathrm{adv.}}$ (advective heat), and $Q_{\mathrm{turb.}}$ (turbulent heat), lead to a change in temperature within bedrock ΔT. Unloading due to loss of glacier or rock mass leads to a change in the stress distribution within the rock mass $\Delta\sigma$. Both ΔT and $\Delta\sigma$ influence local hydrogeology in permafrost rock, favoring the buildup of hydrostatic pressure $P_{\mathrm{H_2O}}$ within fractures. All of the aforementioned changes (i.e., $+\Delta T$, $-\Delta\sigma$, $+P_{\mathrm{H_2O}}$) negatively affect the mechanical shear strength of geological discontinuities. The thick blue and red lines indicate cold- and warm-based glacier conditions, respectively. The dashed black line indicates the basal shear plane, while $h_{\mathrm{H_2O}}$ illustrates the local water table. $\Delta\boldsymbol{a}$ represents the acceleration of the rock mass triggered by the combined effects described above.

observed the loss of the conjunction to the Southern Bliggferner Glacier in the period 1969 to 2003. This led to the exposure of a ridge with S-oriented rock slabs to direct solar radiation ($Q_{\text{rad.}}$) and to an accelerated conductive warming of rock. Shortly before the failure, basal warm ice is likely to be found to a greater extent at the lower altitudes and to a smaller extent at the higher altitudes in the area of the S-exposed ridge and the Southern Bliggferner Glacier. Basal cold ice is most probable in the upper part of the Northern Bliggferner Glacier and is likely to be framed between warm-ice compartments in the years shortly before failure. Near-surface permafrost indicates cold-ice compartments in close proximity and is evident in the N-oriented rock faces above 3200 m in proximity to the Northern Bliggferner Glacier, as shown by GST and field observations. Cold ice is likely to be absent in the area of the Southern Bliggferner Glacier due to the exposure of the glacier to solar radiation and infiltrating meltwaters from the steep west-facing couloirs above.

Secondly, the distribution of mountain permafrost with low ice content strongly depends on altitude, aspect, slope, terrain roughness, duration, and thickness of insulating snow or glacier ice and vegetation cover and on the inherited thermal signals of large rock mass storing the transient temperature effects of Holocene timescale according to Noetzli and Gruber (2009). More than 80 % of the failed rock mass was thermally insulated by glacier ice before the failure, whereas the steep surface of the west-facing mountain flank underneath allowed undamped air temperature signals to penetrate the rock. Owing to the three-dimensional situation, permafrost is likely to be irregularly shaped due to the complex topography along with heterogeneity in snow and ice cover, resulting in varying ground surface temperatures (Haberkorn et al., 2015). Nevertheless, the warming of air at the study site since the Little Ice Age, and especially in the last decades, is likely to have driven the lower base of the mountain permafrost to higher elevations by conductive heat transport (Biskaborn et al., 2019). In addition, the presence of abundant surface water strongly modifies the shape of permafrost. Advective heat, transported by percolating waters, is an effective mechanism for degrading cleft ice and creating thaw corridors in fractured rock mass (Gruber and Haeberli, 2007; Hasler et al., 2011). In fractured aquifer systems, water flows primarily along fractures, while the intact rock matrix exhibits minimal hydraulic conductivity (K for low-porosity rock is generally in the range of 10^{-8} to $10^{-10}\,\text{m}\,\text{s}^{-1}$). Linked thaw corridors create wedges that induce bottom-up permafrost degradation under saturated conditions and lead to accelerated deepening of permafrost (Magnin and Josnin, 2021). Moreover, rainwater or meltwater heated by the flow over sun-exposed rock slabs are sources of water with temperatures above 0 °C, contributing to an accelerated cleft-ice degradation ($Q_{\text{adv.}}$). The ridge forming the head scarp and the west-facing rock couloirs above the Southern Bliggferner Glacier exhibit conditions that favor the infiltrating of such pre-heated water at the elevation of the detachment zone. The temperature of glacier or snow meltwater is typically 0 °C, considering short travel times. In this case, advective heat transport is less effective for cleft-ice degradation, as part of the water refreezes while infiltrating into the ground. The small gradient between water and ice or rock temperature substantially delays the process of the degradation of ice (Cuffey and Paterson, 2010). It is notable to mention that both hydrostatic water pressure and solute concentration are not very effective in lowering the melting point for the purpose of cleft-ice degradation in alpine environments due to the high water pressure (equal to 1000 m in hydraulic head) or high water molality ($0.54\,\text{mol}\,\text{kg}^{-1}$) that are required in order to lower the melting point by -1 °C in temperature (Krautblatter, 2010). Thirdly, the system feedback of basal glacier warming leading to meltwater production and subsequent loss in permafrost underneath incorporates a highly simplified view in our model. Permafrost might outlast several decades or centuries when being fed with cold water around 0 °C. The permeability of fractured rock slopes affected by permafrost is mainly influenced by the properties of the fractured rock aquifer – fracture density, persistence, aperture and fracture infills, and the interconnectivity of the fracture system (Hakami, 1995) – and by the presence of ice-sealed discontinuities as features of permafrost (Woo, 2012). The permeability of ice-sealed fractures in granite was found to be 1 to 3 orders of magnitude lower in comparison to the thawed state (Pogrebiskiy et al., 1977). The spatial contrast in permeability due to (i) the cluster of ice-sealed and ice-free fractures; (ii) varying system connectivity, fracture apertures, and geometries of geological structures such as bedding or foliation, joints, and fault zones; or (iii) the strong gradient of weathering that reduces with higher depths in combination with high surficial water discharge might lead to the buildup of localized hydrostatic water pressures ($P_{\text{H}_2\text{O}}$ at individual fractures). Hydraulic heads of several decameters were derived for individual fractures within permafrost rock at Zugspitze (Germany). While extreme precipitation events led to hydraulic heads of 40 ± 10 m, average daily snowmelt resulted in 27 ± 6 m according to Scandroglio et al. (2024).

Despite the rather slow process of permafrost degradation, given infiltrating meltwater of 0 °C, the permeability of rock mass, including ice-sealed discontinuities, can be increased by other mechanisms, which are described below.

– Pre-failure activity, as observed at many high-volume rock slope instabilities in permafrost (Caduff et al., 2021; Hilger et al., 2021; Etzelmüller et al., 2022), is indicated by continuous or accelerated movements of parts within the susceptible rock slope or even the entire slope and may affect local hydrogeology via the creation of new fractures and voids. As a result of glacial thinning and the observed debris flows in the faces underneath the Bliggspitze rock slope, the local stress field changes in response to glacier or rock debuttressing

($\Delta\sigma$) and may therefore create new fractures or initialize small movements that indicate pre-failure activity.

– Water pressure can mechanically widen the fracture aperture, challenging the tensile strength of potential ice-infillings and enabling localized channeling of water to higher depths by changes in hydraulic aperture. According to the cubic law for fluid flow, hydraulic conductivity is proportional to the cube of the fracture aperture (Witherspoon et al., 1980), meaning small changes in aperture significantly affect hydraulic conductivity. Hydraulic packer tests conducted in a sparsely fractured granite within boreholes at the underground research tunnel of the Korea Atomic Energy Research Institute (KAERI) could show a distinct increase in fracture aperture at relatively low hydraulic pressure. An applied hydraulic head of 20 m (50 m) resulted in a change in fracture aperture by a factor of 1.22 (1.44) on average (Ji et al., 2013). Hydrostatic water pressure influences effective normal stresses, which increase the permeability of fractures due to the nonlinear closure behavior of the fracture aperture, especially under low normal stresses Zangerl et al. (2008). Alternatively, shear dilatation, likely to be favored by the influence of hydrostatic water pressure, increases permeability by changing the channel geometry, concentrating the flow path along these fractures (Min et al., 2004).

There are certain indications that pressurized, cold water encountering ice-infillings in joints under turbulent water flow ($Q_{\text{turb.}}$) might create scours in the ice via mechanic erosion due to the contact with water vortexes (similar to the creation of moulins within the glacier). Viscous dissipation from turbulence generates heat, increasing temperature gradients and potentially accelerating ice degradation. Turbulency, influenced by flow velocity and stream geometry, is more likely to occur in highly connected, fractured rock masses exposed to periglacial weathering and under high water pressure resulting from glacier discharge. These effects may be limited to shallow depths and are challenging to quantify in natural conditions. The impact of turbulence on cleft-ice degradation and the subsequent increase in permeability is believed to be relatively insignificant when compared to the previously discussed mechanism.

Considering basal water discharge of glaciers in spring and summer, a temporary rise in the water table is likely to occur up to the elevation of the PDL. Although permafrost may last longer given the discharge of glacial meltwater, it is most likely that water will infiltrate to greater depths along preferred high-permeability pathways whether permafrost is present or not. Hydrogeology in fractured permafrost rock mass is still scarcely researched and is explained mainly by conceptual considerations rather than by real in situ observations.

5.2 Mechanical analysis of Bliggspitze rock slope failure and implications of results

5.2.1 Structural predisposition and limitations of the modeling framework

Rock slope failures in brittle fractured rock are governed by shearing along pre-defined discontinuities (Eberhardt et al., 2004; Brideau et al., 2009; Welkner et al., 2010). As the UDEC framework does not allow for arbitrary crack propagation through intact blocks and enables shearing only along explicitly defined discontinuities, all geometrical structures are integrated as fully persistent structures. Rock bridges are considered by the cohesive term within the Mohr–Coulomb shear criterion that was assigned to all discontinuities (see comparable rock mechanic studies, i.e., Fischer et al., 2010; Gischig et al., 2011; Mamot et al., 2021). Unlimited slope displacement, indicating total rock slope failure, could only be represented by explicitly modeling discontinuities that are dipping out of the slope and allowing for kinematic freedom of the blocks. Therefore, the integration of the basal shear zone was essential to enable total failure in the UDEC simulations.

Given the geologically predisposed state of a rock slope, altered by hydro-thermomechanical forcings over multiglacial cycles as described by Grämiger et al. (2018, 2020), the here-conducted mechanical modeling study emphasizes the analysis of the final triggering event leading to the failure and the formation of a fully persistent shear zone. In order to generate a model representing the pre-failure state of the Bliggspitze rock slope in the decades before the failure, we ran sensitivity tests on shear parameters of discontinuities and structural geometry to determine a critical but stable state (see scenario S1). The hypothesized pre-failure state can be described by various combinations of friction angle and cohesion. It can be interpreted in terms of characteristics of the basal shear zone, as this structural feature had the main control on rock slope displacement. The chosen pair of shear parameters of $\phi = 30$ and $c = 0.1$ MPa indicate an overall low shear strength of the rupture surface, which is possibly attributed to weathered material, foliation orientation, and tectonically stressed and deformed structures within the gneissic rock mass. For reference, the low friction angle ϕ is slightly higher than tested residual friction angles of brittle fault zone material $\phi_{\text{res.}} = 25.7$ to $28.9°$ (Strauhal et al., 2017), while the cohesion c leads to the conclusion of a low proportion of intact rock bridges.

We argue that the basal shear zone follows a sequence of steeply inclined fault zones and aligns with the orientation of articulated foliation in the lower part of the slope. The modeled foliation does not impact the slope instability but was modeled only by straight-line structures (see scenario S1 geometry C in Table 3). As observed at the field site, the foliation of rock mass follows the southern limb of the N–S-oriented tectonic synform at the rock slope and is slightly

bent. On the opposite side of the valley from the Bliggspitze rock slope, morphology exhibits extended rock slabs following the tectonic structure of the northern limb of the synform. The tectonic setting suggests that discontinuities following the foliation pattern dip out at the lower toe of the slope, favoring the development of a continuous and curved basal shear zone.

5.2.2 Mechanical response to a changing cryosphere

S2 – Glacier unloading. Glacial unloading indicates a limited impact on rock slope displacement that varies in the range of 0.03 to 0.08 m, as modeled for the Bliggspitze rock slope. The glacier was modeled as an elastoplastic material, creating the lowest possible shear resistance to the adjacent intruding rock mass. This was consistent with findings of McColl and Davies (2013) and Grämiger et al. (2017), who concluded that a glacier acts as poor buttress due to the ductile behavior of ice under small strain. We divided the glacier into an upper and a lower part. The results proved the mechanical logic that load applied to the upper part of the rock slope only leads to the highest simulated displacement (Fig. 14: stage 9), whereas load applied to the lower part only leads to the lowest displacement (stage 0 – buttress effect).

Modeling both the upper and lower part of the glacier, the results indicate mixed effects attributed to (i) unloading and (ii) to inertia or the selected material model of the lower glacier covering the outcrop of the basal shear zone and affecting unhindered sliding of the failing rock slope. The latter is an inherent effect of UDEC mechanics imposed by the approach of modeling the glacier under a stationary geometry with elastoplastic material. As the focus is on rock slope mechanics rather than glacier ice deformation, the applied material properties were limited to a lower boundary in order to prevent the glacier from freely deforming under its own weight, while also concentrating on displacements within the rock mass. In contrast, other UDEC studies with a similar modeling approach have shown a pronounced effect on rock slope displacement for retreating valley glaciers (Fischer et al., 2010; Rechberger and Zangerl, 2022). They differ from the Bliggspitze study site by considering a higher change in glacier thickness of more than 100 m, and both of them have in common that slope failure occurred when the slope was almost free of ice.

Despite the aforementioned handicap in the modeling approach and the lack of ability to recreate the results of comparable studies, we hypothesize that mass loss of the Northern Bliggferner Glacier was one of several factors preparing the rock slide. Firstly, the Northern Bliggferner Glacier lost several decameters of ice in the lower part while remaining stagnant in the upper part between 1970 and 2003 (Sommer et al., 2023; see Fig. 5). Secondly, the relatively rapid changes in the stress field lead to stress redistribution and are likely to affect crack propagation and failure initiation, including the failure of rock bridges, via sub-critical fracture propagation (Atkinson, 1982).

S3 – Permafrost distribution and its effect on deep-seated shear planes. By iteratively incrementing the mountain permafrost altitude, the resulting rock slope displacement increased from a minimum of about 0.01 m to a maximum of 0.05 m (see Fig. 15). We applied a highly simplified permafrost model by (i) distinguishing only between frozen and unfrozen areas, (ii) assuming uniform distribution delineating unfrozen and frozen areas by a horizontal line, (iii) neglecting active-layer dynamics, and (iv) accounting for permafrost by increasing the shear strength of all discontinuities within the frozen area using synthetic values that derived from theoretical considerations of rock and ice mechanics as proposed by Krautblatter et al. (2013).

To date, the influence of permafrost on the mechanics of deep-seated shear zones located at depths > 30 m, as in the case of the Bliggspitze rock slope, is poorly understood. In contrast to shallow shear planes, where ice-infillings control shear strength dependent on the thermal state (Mamot et al., 2018, 2020), rock–rock contacts of joints may suppress the effect of ice-infillings at higher normal load. Moreover, low deformation rates favor the creep of ice which does not affect overall shear strength under low strain (Hobbs, 2010). At deep-seated shear planes and zones under warming permafrost, the effect of ice-infillings on overall shear strength might be minor, but mechanical degradation of intact rock bridges become more relevant, as intact rock properties are also affected by rising temperatures (Mellor, 1973; Inada and Yokota, 1984; Draebing and Krautblatter, 2012).

In scenario S3A, we assigned a surplus in friction angle $\Delta\phi = +5^\circ$ to frozen discontinuities derived by the results on frozen and unfrozen shear tests at normal stress in the range of 0.6 to 1.3 MPa, equivalent to depths of the shear plane of 25 to 50 m (Krautblatter et al., 2013). In scenario S3B, we additionally considered the mechanical degradation of rock bridges by attempting to incorporate insights from the conducted tensile strength tests under frozen and unfrozen states. However, the actual distribution and quantity of rock bridges is unknown, leading to a blurred view on how to translate the results into the Mohr–Coulomb shear as suggested by the concept of Kemeny (2003). Further research and verification of the model utilized in this study are essential for a comprehensive understanding of the mechanics of deep-seated shear planes in permafrost.

S4 – Peak groundwater level. The modeled pre-failure state of the Bliggspitze rock slope proved to be hypersensitive to changes in groundwater level. Total failure occurred when the lower outcrop of the basal shear zone was exceeded by the groundwater table. In addition, we used a reverse modeling approach, asking which shear parameters would allow the model to remain stable given a defined peak groundwater level at an elevation of 3050 m a.s.l., which corresponds to the center of gravity of the failing rock mass. In order to ensure stable conditions, the shear properties must in-

crease by $\Delta\phi = +10° \Delta c = +0.2$ MPa in comparison to the pre-failure state, suggesting a pronounced destabilizing effect of hydrostatic water pressure on slope stability, which was also reported by other UDEC studies in periglacial environments (Fischer et al., 2010; Stoll, 2020). For the given reverse modeling state, a hydrostatic water pressure of approximately 0.5 MPa acted on the basal shear zone, counteracted the weight of the rock mass above, and asserted pressure gradients on joint walls within inclined and vertical discontinuities.

In the case of the Bliggspitze rock slope, peak groundwater levels can result from transient peak discharge of meltwater or intense liquid precipitation (Magnusson et al., 2014) or abrupt release from englacial stored water (Fountain and Walder, 1998). Although the hydraulic conductivity of the rock slope was not quantified, we assumed fully saturated conditions to exist due to the imbalance of high peak discharge versus an assumed limited infiltration capacity. The state of transient peak groundwater level was simulated by a static, unconfined water table, defined by the elevation of PDL and the bedrock's surface topography below the warm glacier base (Fig. 12). In contrast to Grämiger et al. (2020), who stated that basal water pressure could reach values close to the pressure of ice overburden, we neglected the effect of subglacial water pressure at the base of the glacier due to the small thickness of the overlying glacier and the geometry of slope favoring surficial runoff at the glacier base.

5.3 Permafrost characterization and interpretation

GST records display heterogeneity that is most likely attributed to differences in locations of measurements, which would account for the variability in snow depth and annual duration of snow cover (daily standard deviation of GST measurement as interpreted by Haberkorn et al. (2015) and Draebing et al. (2022), Fig. 6) and for the microscale roughness of topography and aspect (see Fig. 1). The surface of the rock slope is characterized by blocky, heavily weathered rock, which is distributed in a debris-like soil layer over the fractured rock mass below. This layer contains a high proportion of voids. Therefore, direct solar radiation may be less efficient at warming the rock mass because cold air trapped in voids acts as additional buffer. The measured GST, elevation, aspect, and the high content of voids collectively support the favorable conditions for the existence of permafrost in the area of the head scarp of the Bliggspitze rock slope failure.

The ERT measurement conducted on the fragmented rock mass 2 years after failure indicates permafrost-free conditions and water-saturated areas in the lower part of the transect according to the interpretation logic applied in other ERT-studies (Krautblatter and Hauck, 2007; Keuschnig et al., 2017; Offer et al., 2024). The unusual finding is that if the glacier covering the rock mass exhibited warm ice at its bed before failure, meltwater infiltration might have eroded the preexisting permafrost under cold-based conditions (the mechanism was discussed above). If permafrost was still there upon failure, frictional energy dissipation caused by the rock slide and fragmentation of rock mass (Erismann and Abele, 2001) might have eroded permafrost within the area of the affected mass movement.

Water outlets' measured high electrical conductivity values at nearby springs could be used as an indicator for active-layer deepening (Colombo et al., 2018) or ongoing glacier erosion (Collins, 1979) depending on the source the water is stemming from. In the area surrounding the Bliggspitze rock slide, groundwater mineralization could be influenced by landslide activity (Bogaard et al., 2007). However, it is unlikely that the higher measured conductivity is attributed to tailing effects related to rock slope failure that occurred 4 years before. If recent landslide activity, glacier, or rock glacier influence could be excluded as a source for mineralized water, we inferred the water source to be permafrost. Therefore, we interpret the observed dense cluster of springs with high electrical conductivity below the Bliggspitze rock slope as active-layer deepening and loss of permafrost.

5.4 Implications of frozen rocks on mechanics of deep-seated shear planes and anisotropic rock fabric

The laboratory experiments are designed to investigate tensile strength for frozen and unfrozen states of brittle intact rock (to account for mechanical degradation of rock bridges under thawing permafrost) and to analyze the structural control of the foliation.

Rock bridges can be incorporated into the Mohr–Coulomb shear criterion through the use of the cohesive term, represented by the parameter of fracture toughness mode II and geometry (Kemeny, 2003). As the results of the Brazilian test are linearly related to fracture toughness mode II (Hua et al., 2017) and require less expensive sample preparation, we have elected to utilize the Brazilian test. The results of the conducted BZTs clearly demonstrate higher values for frozen than unfrozen rock samples. Consequently, we argue that permafrost can increase overall shear strength, even for deep-seated shear planes, by increasing the shear strength of individual rock bridges, regardless of the presence of ice-infillings.

The results of the BZT do not indicate that the foliation of intact rock is structurally controlling the rock slope mechanics. The two extreme cases (parallel and perpendicular sample arrangement) indicate dependence on foliation, which is more pronounced for the frozen than for the unfrozen sample group. Given the limited number of samples tested ($n = 6$ or 7), the observed variation within each case, which was at least 4.5 MPa, the variation is primarily attributed to the natural heterogeneity of the samples. Additionally, the observation that fracturing occurred along the defined area spanned by the opposing load bridges, regardless of the orientation of foliation, indicates that the tested paragneiss can be de-

scribed as a rather isotropic material. Apart from the existing foliation-parallel joints, which define distinct shear planes, test results suggest that anisotropy of rock fabric in intact rock is mechanically irrelevant for the Bliggspitze rock slope failure.

The increase in σ_t from an unfrozen state at $T = +20\,°C$ to a frozen state at $-10\,°C$ of $+65.8\%$ is distinctly higher than the findings of comparable studies. Mellor (1973) reported an increase from an unfrozen state ($+23\,°C$) to a frozen state ($-8\,°C$) of approximately $+8.4\%$ for saturated granite. Inada and Yokota (1984) reported an increase from an unfrozen state (T_{room}) to a frozen state ($-40\,°C$) of $+70.1\,\%$ for saturated granite. In contrast to commonly applied constant strain, we manually simulated constant stress tests and reduced the time to perform a single test. We hypothesize that the quick increase in applied load restricts the possibility of ice relaxation or degradation and sample deformation before reaching peak tensile strength. Thus, the performed tests result in higher tensile strength values compared to previous studies.

It is of interest to note that the test results pertain to areas within the geological unit that exhibit greater strength and are more resistant to erosion. When collecting samples, besides homogeneity and lithology, accessibility and transportation were criteria for choosing a site. Samples were taken from block streams with low fine-grain content, indicating periglacial phenomena in a relict state Oliva et al. (2023). In these circumstances, blocks found on top of the block stream today represent the most weathering-resistant parts.

5.5 Synthetic discussion

The Bliggspitze rock slide is an example of a hitherto underexplored but commonly occurring phenomenon resulting from cascading effects posed by the regime shift in polythermal glaciers. The Northern Bliggferner Glacier covered the rock slope before the failure. More than $3.9 \times 10^6\,m^3$ of rock and ice were mobilized by the first-time formation of the rock slide in 2007. The rock slope was mechanically impacted by changes in the cryosphere, culminating in the formation of the basal shear zone and several slabs. The creation of a persistent shear zone was favored by the orientation of fault zones and the foliation of the paragneissic rock slope. While multiple processes contributed to the destabilization of the Bliggspitze rock slope, water infiltration due to the increase in the polythermal dividing line and crevasse opening led to the buildup of hydrostatic pressure in the rock mass on a large and zonally limited scale, suggesting the strongest trigger for the first-time formation of the rock slide.

The Bliggspitze rock side is not believed to be a singular case. The recent rock slope failure at Piz Scerscen in Switzerland on 14 April 2024 showed characteristics similar to the Bliggspitze rock slide presented here. The affected failure volume of the bedrock was roughly estimated to be about $5 \times 10^6\,m^3$ (PERMOS, 2024), the west-facing mountain flank is situated in the ice-poor permafrost zone (Kenner et al., 2019) and was previously covered by glacier ice. Before the failure, an anomalous period of warm April weather occurred. The failure scarp exhibited wet patches most likely attributed to zonal infiltration of water. Similar conditions, a warm weather period prior to the failure, and wet areas at the failure scarp have been observed for the Mount Steller rock–ice avalanche too (Huggel et al., 2008).

A further prominent example of a mass movement induced by the thermal regime change of a glacier and dynamics of the subglacial hydrology is the severe collapse of the Marmolada Glacier (Italy) in June 2022. Although the detachment occurred at the glacier–bedrock interface and primarily affected the glacier ice, the processes leading to the failure are similar to the combined rock slope and glacier failures observed at Bliggspitze and Piz Scerscen. Chiarle et al. (2023) hypothesized that the Marmolada Glacier collapse was triggered by the buildup of water pressure at the temperate ice–bedrock interface, while the cold glacier margins hindered water outflow.

Water may not solely act as a trigger for large slope instabilities in cryospheric environments. The abundant amount of water stored not only in liquid form but also in the solid forms of snow and ice substantially increases run-out length and impacts the mechanics of the propagating rock avalanches, as observed in the rock slope failures of Mount Chamoli (India) in 2021 (Shugar et al., 2021), Fluchthorn (Austria) in 2023 (Krautblatter et al., 2024), and Piz Scerscen (Switzerland) in 2024. Concomitant with climate warming, we expect further large slope instabilities as higher areas undergo paraglacial transition. Regardless of triggering the failure or increasing its cascading effects, the analysis of water, ice, and snow availability is substantial in anticipating large rock slope failure in alpine cryosphere.

6 Conclusion

In this study, we developed a conceptual model explaining the uplift of the cold–warm dividing line of polythermal glaciers concomitant to climate warming as a result of the holistic observations of the current and past state of the cryosphere at the field site. A shift in the polythermal dividing line (PDL), a term first defined in this paper, poses thermal and hydrological implications for the rock slope underneath the glacier, thereby challenging its mechanical stability. We simulated the mechanical impact on the rock slope during a regime shift in the polythermal Northern Bliggferner Glacier considering glacier mass loss, changing mechanical properties of frozen and unfrozen discontinuities, and adaption of the hydrogeological situation. To complement the mechanical framework of deep-seated shear planes and zones in permafrost, we tested the tensile strength of anisotropic

paragneiss at frozen and unfrozen states. The main findings of the study are presented below.

- Dynamics of glaciers, permafrost, and hydrogeology are strongly interlinked. The Bliggspitze rock slide can be described as a failure type prepared and triggered by these interlinked dynamics. The hydro-mechanical simulations reveal that different processes (glacier unloading, permafrost degradation, rise in groundwater table) affect rock slope stability to different magnitudes. However, the combination of several simultaneous processes still appears to be the most effective method for destabilizing rock slopes, leading to a progressive failure mechanism.
- The most intense impact on destabilizing glacier-covered rock slopes over a short time period results from the shifting of a polythermal glacier towards a temperate regime and its hydrogeological implications. The infiltration of water below areas that were previously sealed with cold glacier ice substantially alters hydrogeological conditions. As a consequence of snowmelt, glacier meltwater, or rainfall, transient buildup of hydrostatic water pressure in the fracture network may eventually trigger slope failures.
- Glacial unloading affects overall slope stability via the change in the in situ stress field. Stress redistribution leads to crack propagation and can peak with the onset of shearing or even total rock slope failure. Although our model could not prove a distinct decrease in stability via the simulation of glacier unloading due to inherent limitations of the setup, we found that the rock slope was highly susceptible to glacier erosion, i.e., the removal of rock at the toe of the slope.
- Permafrost thaw destabilizes large rock slides with deep-seated shear zones via mechanical degradation of rock bridges and the consequences this imposes on the local hydrogeology. Ice-filled fractures are less permeable than ice-free fractures, and the degradation of ice-infillings additionally releases stored water.
- Tensile strength serves as a proxy for representing the strength of rock bridges in a Mohr–Coulomb shear criterion. It has been demonstrated here that the tensile strength of foliated paragneiss is highly dependent on the frozen or unfrozen state, whereas the foliation orientation has a minor effect on tensile strength.
- Smaller pre-failure events and a warm climate in the months leading up to the failure, which peaked at a historical temperature record, preceded the main failure event at Bliggspitze on 29 June 2007. The timing of the failure coincides with the daily peak river discharge temperature recorded at the Vernagtferner Glacier in close proximity to the event.
- The high electrical conductivity measured at springs below the Bliggspitze rock slide indicates permafrost degradation, as geomorphic analysis has excluded rock glaciers as a water source. The loss of cold ice, such as the observed loss of ice aprons in steep faces above the Northern Bliggferner Glacier, has been visually documented from 1969 to 2003. Regarding elevation, aspect, and measured ground surface temperatures, the head scarp resulting from the failure is situated in permafrost-favorable terrain.

Code availability. The authors declare that the code used in this study is available upon reasonable request. Interested researchers can contact the corresponding author to obtain access to the code.

Data availability. The authors declare that the data used in this study are available upon reasonable request. Interested researchers can contact the corresponding author to obtain access to the data.

Supplement. The supplement related to this article is available online at: https://doi.org/10.5194/esurf-13-41-2025-supplement.

Author contributions. FP wrote the manuscript, conducted the data analysis, and drafted the concept for the UDEC modeling study. SW acted as co-pilot and mentor throughout the processes of developing the paper structure and provided essential help toward improving the manuscript. JS conducted the tensile strength tests in the laboratory. CZ contributed to framing the setup of the mechanical modeling study and helped to revise the draft of the manuscript. CF recorded the ground surface temperature data used in this study. JF wrote text regarding the analysis of the Northern Bliggferner Glacier. MK initiated the main concept and the first framework for the paper and conducted the ERT measurements in 2009.

Competing interests. At least one of the (co-)authors is a member of the editorial board of *Earth Surface Dynamics*. The peer-review process was guided by an independent editor, and the authors also have no other competing interests to declare.

Disclaimer. Publisher's note: Copernicus Publications remains neutral with regard to jurisdictional claims made in the text, published maps, institutional affiliations, or any other geographical representation in this paper. While Copernicus Publications makes every effort to include appropriate place names, the final responsibility lies with the authors.

Acknowledgements. The authors would like to thank Martin Stocker-Waldhuber and Michael Kuhn for providing access to the DHM69 dataset and to Christian Sommer for providing the glacier thickness model. In addition, we thank Karl Krainer for pro-

viding the publication containing the mapping and measurements of springs. Felix Pfluger expresses special thanks to Maike Offer for proofreading sections of the manuscript and providing support with the ERT analysis, and to Benjamin Jacobs for the inspiration for the laboratory setup. Felix Pfluger also thanks Sebastian Westermann for the stimulating discussions on heat transport mechanisms in relation to permafrost degradation. We extend our sincere thanks to reviewers Philip Deline and Reginald Hermanns, and to the handling editor Dirk Scherler, for their valuable efforts and constructive feedback.

Financial support. This research has been supported by the Bayerisches Staatsministerium für Wissenschaft und Kunst (grant no. M3OCCA).

Review statement. This paper was edited by Dirk Scherler and reviewed by Reginald Hermanns and Philip Deline.

References

Atkinson, B. K.: Subcritical crack propagation in rocks: theory, experimental results and applications, J. Struct. Geol., 4, 41–56, https://doi.org/10.1016/0191-8141(82)90005-0, 1982.

Ballantyne, C. K.: Paraglacial geomorphology, Quaternary Sci. Rev., 21, 1935–2017, 2002.

Ballantyne, C. K., Sandeman, G. F., Stone, J. O., and Wilson, P.: Rock-slope failure following Late Pleistocene deglaciation on tectonically stable mountainous terrain, Quaternary Sci. Rev., 86, 144–157, https://doi.org/10.1016/j.quascirev.2013.12.021, 2014.

Biskaborn, B. K., Smith, S. L., Noetzli, J., Matthes, H., Vieira, G., Streletskiy, D. A., Schoeneich, P., Romanovsky, V. E., Lewkowicz, A. G., Abramov, A., Allard, M., Boike, J., Cable, W. L., Christiansen, H. H., Delaloye, R., Diekmann, B., Drozdov, D., Etzelmüller, B., Grosse, G., Guglielmin, M., Ingeman-Nielsen, T., Isaksen, K., Ishikawa, M., Johansson, M., Johannsson, H., Joo, A., Kaverin, D., Kholodov, A., Konstantinov, P., Kröger, T., Lambiel, C., Lanckman, J.-P., Luo, D., Malkova, G., Meiklejohn, I., Moskalenko, N., Oliva, M., Phillips, M., Ramos, M., Sannel, A. B. K., Sergeev, D., Seybold, C., Skryabin, P., Vasiliev, A., Wu, Q., Yoshikawa, K., Zheleznyak, M., and Lantuit, H.: Permafrost is warming at a global scale, Nat. Commun., 10, 264, https://doi.org/10.1038/s41467-018-08240-4, 2019.

Bogaard, T., Guglielmi, Y., Marc, V., Emblanch, C., Bertrand, C., and Mudry, J.: Hydrogeochemistry in landslide research: a review, B. Soc. Géol. Fr., 178, 113–126, 2007.

Brideau, M.-A., Yan, M., and Stead, D.: The role of tectonic damage and brittle rock fracture in the development of large rock slope failures, Geomorphology, 103, 30–49, 2009.

Caduff, R., Strozzi, T., Hählen, N., and Häberle, J.: Accelerating landslide hazard at Kandersteg, Swiss Alps; combining 28 years of satellite Insar and single campaign terrestrial radar data, Understanding and Reducing Landslide Disaster Risk: Volume 5 Catastrophic Landslides and Frontiers of Landslide Science 5th, 267–273, https://doi.org/10.1007/978-3-030-60319-9_29, 2021.

Chiarle, M., Viani, C., Mortara, G., Deline, P., Tamburini, A., and Nigrelli, G.: Large glacier failures in the Italian Alps over the last 90 years, Geogr. Fis. Din. Quat., 45, 19–40, 2023.

Chimani, B., Matulla, C., Böhm, R., and Hofstätter, M.: A new high resolution absolute temperature grid for the Greater Alpine Region back to 1780, Int. J. Climatol., 33, 2129–2141, https://doi.org/10.1002/joc.3574, 2013.

Collins, D. N.: Hydrochemistry of meltwaters draining from an alpine glacier, Arct. Alp. Res., 11, 307–324, 1979.

Colombo, N., Salerno, F., Gruber, S., Freppaz, M., Williams, M., Fratianni, S., and Giardino, M.: Review: Impacts of permafrost degradation on inorganic chemistry of surface fresh water, Global Planet. Change, 162, 69–83, https://doi.org/10.1016/j.gloplacha.2017.11.017, 2018.

Cruden, D. M. and Varnes, D. J.: Landslide Types and Processes, Transportation Research Board, U.S. National Academy of Sciences, Special Report, 247: 36-75, Special Report – National Research Council, Transport. Res. B., 247, 36–57, 1996.

Cuffey, K. M. and Paterson, W. S. B.: The physics of glaciers, Academic Press, https://doi.org/10.3189/002214311796405906, 2010.

Davies, M. C., Hamza, O., and Harris, C.: The effect of rise in mean annual temperature on the stability of rock slopes containing ice-filled discontinuities, Permafrost Periglac., 12, 137–144, 2001.

Dejean de la Bâtie, J.: Ingenieurgeologische und hydrogeologische Untersuchung der Massenbewegung im Bereich der Bliggspitze im Ötztal-Stubai-Kristallin (Kaunertal, Tirol), MS thesis, University of Innsbruck, Faculty of Geo- and Atmospheric Sciences, 159 pp., 2016.

DIN-EN-13755:2008-08: Prüfverfahren für Naturstein- Bestimmung der Wasseraufnahme unter atmosphärischem Druck, Deutsche Fassung EN 13755:2008, Beuth Verlag GmbH, Berlin, Germany, https://doi.org/10.31030/1438560, 2008.

Draebing, D. and Krautblatter, M.: P-wave velocity changes in freezing hard low-porosity rocks: a laboratory-based time-average model, The Cryosphere, 6, 1163–1174, https://doi.org/10.5194/tc-6-1163-2012, 2012.

Draebing, D., Krautblatter, M., and Dikau, R.: Interaction of thermal and mechanical processes in steep permafrost rock walls: A conceptual approach, Geomorphology, 226, 226–235, https://doi.org/10.1016/j.geomorph.2014.08.009, 2014.

Draebing, D., Mayer, T., Jacobs, B., and McColl, S. T.: Alpine rockwall erosion patterns follow elevation-dependent climate trajectories, Commun. Earth Environ., 3, 21, https://doi.org/10.1038/s43247-022-00348-2, 2022.

Eberhardt, E., Stead, D., and Coggan, J.: Numerical analysis of initiation and progressive failure in natural rock slopes—the 1991 Randa rockslide, Int. J. Rock Mech. Min., 41, 69–87, 2004.

Erismann, T. H. and Abele, G.: Dynamics of rockslides and rockfalls, Springer Science & Business Media, ISBN 3540671986, 2001.

Escher-Vetter, H., Braun, L. N., and Siebers, M.: Hydrological and meteorological records from the Vernagtferner Basin – Vernagtbach station, for the years 2002 to 2012, PANGAEA [data set], https://doi.org/10.1594/PANGAEA.829530, 2014.

Etzelmüller, B. and Hagen, J. O.: Glacier-permafrost interaction in Arctic and alpine mountain environments with examples from southern Norway and Svalbard, in: Cryospheric Systems: Glacier and Permafrost, edited by: Harris, C. and Murton, J. B., vol.

242, Geological Society, London, Special Publications, 11–27, https://doi.org/10.1144/GSL.SP.2005.242, 2005.

Etzelmüller, B., Czekirda, J., Magnin, F., Duvillard, P.-A., Ravanel, L., Malet, E., Aspaas, A., Kristensen, L., Skrede, I., Majala, G. D., Jacobs, B., Leinauer, J., Hauck, C., Hilbich, C., Böhme, M., Hermanns, R., Eriksen, H. Ø., Lauknes, T. R., Krautblatter, M., and Westermann, S.: Permafrost in monitored unstable rock slopes in Norway – new insights from temperature and surface velocity measurements, geophysical surveying, and ground temperature modelling, Earth Surf. Dynam., 10, 97–129, https://doi.org/10.5194/esurf-10-97-2022, 2022.

Faillettaz, J., Funk, M., and Vincent, C.: Avalanching glacier instabilities: Review on processes and early warning perspectives, Rev. Geophys., 53, 203–224, https://doi.org/10.1002/2014RG000466, 2015.

Farr, T. G., Rosen, P. A., Caro, E., Crippen, R., Duren, R., Hensley, S., Kobrick, M., Paller, M., Rodriguez, E., Roth, L., Seal, D., Shaffer, S., Shimada, J., Umland, J., Werner, M., Oskin, M., Burbank, D., and Alsdorf, D.: The Shuttle Radar Topography Mission, Rev. Geophys., 45, RG2004, https://doi.org/10.1029/2005RG000183, 2007.

Fischer, A., Seiser, B., Stocker-Waldhuber, M., Mitterer, C., and Abermann, J.: The Austrian Glacier Inventories GI 1 (1969), GI 2 (1998), GI 3 (2006), and GI LIA in ArcGIS (shapefile) format: [dataset publication series], PANGAEA [data set], https://doi.org/10.1594/PANGAEA.844988, 2015.

Fischer, L., Amann, F., Moore, J. R., and Huggel, C.: Assessment of periglacial slope stability for the 1988 Tschierva rock avalanche (Piz Morteratsch, Switzerland), Eng. Geol., 116, 32–43, https://doi.org/10.1016/j.enggeo.2010.07.005, 2010.

Fountain, A. G. and Walder, J. S.: Water flow through temperate glaciers, Rev. Geophys., 36, 299–328, 1998.

Geertsema, M., Menounos, B., Bullard, G., Carrivick, J. L., Clague, J. J., Dai, C., Donati, D., Ekstrom, G., Jackson, J. M., Lynett, P., Pichierri, M., Pon, A., Shugar, D. H., Stead, D., Del Bel Belluz, J., Friele, P., Giesbrecht, I., Heathfield, D., Millard, T., Nasonova, S., Schaeffer, A. J., Ward, B. C., Blaney, D., Blaney, E., Brillon, C., Bunn, C., Floyd, W., Higman, B., Hughes, K. E., McInnes, W., Mukherjee, K., and Sharp, M. A.: The 28 November 2020 Landslide, Tsunami, and Outburst Flood – A Hazard Cascade Associated With Rapid Deglaciation at Elliot Creek, British Columbia, Canada, Geophys. Res. Lett., 49, e2021GL096716, https://doi.org/10.1029/2021GL096716, 2022.

GeoSphere Austria: Bundesanstalt für Geologie, Geophysik, Klimatologie und Meteorologie – Data Hub, https://data.hub.geosphere.at/, last access: 1 November 2023.

Gilbert, A., Vincent, C., Gagliardini, O., Krug, J., and Berthier, E.: Assessment of thermal change in cold avalanching glaciers in relation to climate warming, Geophys. Res. Lett., 42, 6382–6390, https://doi.org/10.1002/2015GL064838, 2015.

Gischig, V., Amann, F., Moore, J. R., Loew, S., Eisenbeiss, H., and Stempfhuber, W.: Composite rock slope kinematics at the current Randa instability, Switzerland, based on remote sensing and numerical modeling, Eng. Geol., 118, 37–53, https://doi.org/10.1016/j.enggeo.2010.11.006, 2011.

Grämiger, L. M., Moore, J. R., Gischig, V. S., Ivy-Ochs, S., and Loew, S.: Beyond debuttressing: Mechanics of paraglacial rock slope damage during repeat glacial cycles, J. Geophys. Res.-Earth, 122, 1004–1036, 2017.

Grämiger, L. M., Moore, J. R., Gischig, V. S., and Loew, S.: Thermomechanical stresses drive damage of Alpine valley rock walls during repeat glacial cycles, J. Geophys. Res.-Earth, 123, 2620–2646, 2018.

Grämiger, L. M., Moore, J. R., Gischig, V. S., Loew, S., Funk, M., and Limpach, P.: Hydromechanical Rock Slope Damage During Late Pleistocene and Holocene Glacial Cycles in an Alpine Valley, J. Geophys. Res.-Earth, 125, e2019JF005494, https://doi.org/10.1029/2019JF005494, 2020.

Gruber, S. and Haeberli, W.: Permafrost in steep bedrock slopes and its temperature–related destabilization following climate change, J. Geophys. Res.-Earth, 112, F02S18, https://doi.org/10.1029/2006JF000547, 2007.

Günzel, F.: Shear strength of ice-filled rock joints, in: Proceedings of the 9th International Conference on Permafrost, Institute of Northern Engineering, University of Alaska Fairbanks, 581–586, ISBN 9780980017922, 2008.

Haberkorn, A., Hoelzle, M., Phillips, M., and Kenner, R.: Snow as a driving factor of rock surface temperatures in steep rough rock walls, Cold Reg. Sci. Technol., 118, 64–75, 2015.

Haeberli, W.: Die Basis-Temperatur der winterlichen Schneedecke als moglicher Indikator fur die Verbreitung von Permafrost in den Alpen, Zeitschrift fur Gletscherkunde und Glazialgeologie, 9, 221–227, 1973.

Haeberli, W.: Investigating glacier-permafrost relationships in high-mountain areas: historical background, selected examples and research needs, in: Cryospheric Systems: Glacier and Permafrost, edited by: Harris, C. and Murton, J. B., vol. 242, Geological Society, London, Special Publications, London, 29–37, https://doi.org/10.1144/GSL.SP.2005.242, 2005.

Hakami, E.: Aperture distribution of rock fractures, PhD thesis, Royal Inst. of Tech, Stockholm, Sweden, ISBN 91-7170-835-9, 1995.

Han, Y., Du, L., and Shen, S.: Study on shear test and shear displacement of frozen joints with different opening degrees, Nat. Hazards, 115, 289–307, https://doi.org/10.1007/s11069-022-05555-w, 2023.

Hasler, A., Gruber, S., Font, M., and Dubois, A.: Advective heat transport in frozen rock clefts: Conceptual model, laboratory experiments and numerical simulation, Permafrost Periglac., 22, 378–389, 2011.

Hermanns, R. L., Schleier, M., Böhme, M., Blikra, L. H., Gosse, J., Ivy-Ochs, S., and Hilger, P.: Rock-Avalanche Activity in W and S Norway Peaks After the Retreat of the Scandinavian Ice Sheet, in: Advancing Culture of Living with Landslides, edited by: Mikoš, M., Vilímek, V., Yin, Y., and Sassa, K., Springer International Publishing, Cham, 331–338, ISBN 978-3-319-53483-1, 2017.

Hiebl, J. and Frei, C.: Daily temperature grids for Austria since 1961 – concept, creation and applicability, Theor. Appl. Climatol., 124, 161–178, https://doi.org/10.1007/s00704-015-1411-4, 2016.

Hiebl, J. and Frei, C.: Daily precipitation grids for Austria since 1961 – development and evaluation of a spatial dataset for hydroclimatic monitoring and modelling, Theor. Appl. Climatol., 132, 327–345, https://doi.org/10.1007/s00704-017-2093-x, 2018.

Hilger, P., Hermanns, R. L., Czekirda, J., Myhra, K. S., Gosse, J. C., and Etzelmüller, B.: Permafrost as a first order control on long-term rock-slope deformation in

(Sub-)Arctic Norway, Quaternary Sci. Rev., 251, 106718, https://doi.org/10.1016/j.quascirev.2020.106718, 2021.

Hobbs, P. V.: Ice physics, Oxford University Press, ISBN 10 019958771X, ISBN 13 9780199587711, 2010.

Hoek, E. and Brown, E. T.: The Hoek–Brown failure criterion and GSI – 2018 edition, Journal of Rock Mechanics and Geotechnical Engineering, 11, 445–463, https://doi.org/10.1016/j.jrmge.2018.08.001, 2019.

Holm, K., Bovis, M., and Jakob, M.: The landslide response of alpine basins to post-Little Ice Age glacial thinning and retreat in southwestern British Columbia, Geomorphology, 57, 201–216, 2004.

Hua, W., Dong, S., Fan, Y., Pan, X., and Wang, Q.: Investigation on the correlation of mode II fracture toughness of sandstone with tensile strength, Eng. Fract. Mech., 184, 249–258, https://doi.org/10.1016/j.engfracmech.2017.09.009, 2017.

Huggel, C., Gruber, S., Caplan-Auerbach, S., Wessels, R. L., and Molnia, B. F.: The 2005 Mt. Steller, Alaska, rock-ice avalanche: A large slope failure in cold permafrost, in: 9th International Conference on Permafrost, INE-UAF, Fairbanks, Alaska, edited by: Kane, D. L. and Hinkel, K. M., International Permafrost Association: Potsdam, 747–752, 2008.

Huggel, C., Clague, J. J., and Korup, O.: Is climate change responsible for changing landslide activity in high mountains?, Earth Surf. Proc. Land., 37, 77–91, 2012.

Hugonnet, R., McNabb, R., Berthier, E., Menounos, B., Nuth, C., Girod, L., Farinotti, D., Huss, M., Dussaillant, I., and Brun, F.: Accelerated global glacier mass loss in the early twenty-first century, Nature, 592, 726–731, 2021.

Inada, Y. and Yokota, K.: Some studies of low temperature rock strength, Int. J. Rock Mech. Min., 21, 145–153, https://doi.org/10.1016/0148-9062(84)91532-8, 1984.

Irvine-Fynn, T. D. L., Hodson, A. J., Moorman, B. J., Vatne, G., and Hubbard, A. L.: Polythermal glacier hydrology: A review, Rev. Geophys., 49, RG4002, https://doi.org/10.1029/2010RG000350, 2011.

Itasca Consulting Group: UDEC – Universal Distinct Element Code, Itasca Software U.S. Minneapolis, United States, https://www.itascacg.com/software/udec (last access: 7 January 2025), 2019.

Ji, S.-H., Koh, Y.-K., Kuhlman, K. L., Lee, M. Y., and Choi, J. W.: Influence of Pressure Change During Hydraulic Tests on Fracture Aperture, Groundwater, 51, 298–304, https://doi.org/10.1111/j.1745-6584.2012.00968.x, 2013.

Kemeny, J.: The Time-Dependent Reduction of Sliding Cohesion due to Rock Bridges Along Discontinuities: A Fracture Mechanics Approach, Rock Mech. Rock Eng., 36, 27–38, https://doi.org/10.1007/s00603-002-0032-2, 2003.

Kenner, R., Noetzli, J., Hoelzle, M., Raetzo, H., and Phillips, M.: Distinguishing ice-rich and ice-poor permafrost to map ground temperatures and ground ice occurrence in the Swiss Alps, The Cryosphere, 13, 1925–1941, https://doi.org/10.5194/tc-13-1925-2019, 2019.

Keuschnig, M., Krautblatter, M., Hartmeyer, I., Fuss, C., and Schrott, L.: Automated electrical resistivity tomography testing for early warning in unstable permafrost rock walls around alpine infrastructure, Permafrost Periglac., 28, 158–171, 2017.

Krautblatter, M.: Detection and quantification of permafrost change in alpine rock walls and implications for rock instability, PhD thesis, Universitäts-und Landesbibliothek Bonn, Germany, https://hdl.handle.net/20.500.11811/4117 (last access: 7 January 2025), 2010.

Krautblatter, M. and Hauck C.: Electrical resistivity tomography monitoring of permafrost in solid rock walls, J. Geophys. Res., 112, F02S20, https://doi.org/10.1029/2006JF000546, 2007.

Krautblatter, M. and Leith, K.: Glacier- and permafrost-related slope instabilities, in: The high-mountain cryosphere, edited by: Huggel, C., Cambridge University Press, 147–165, ISBN 13 978-1-107-06584-0, 2015.

Krautblatter, M., Verleysdonk, S., Flores-Orozco, A., and Kemna, A.: Temperature–calibrated imaging of seasonal changes in permafrost rock walls by quantitative electrical resistivity tomography (Zugspitze, German/Austrian Alps), J. Geophys. Res., 115, F02003, https://doi.org/10.1029/2008JF001209, 2010.

Krautblatter, M., Funk, D., and Günzel, F. K.: Why permafrost rocks become unstable: a rock-ice-mechanical model in time and space, Earth Surf. Proc. Land., 38, 876–887, https://doi.org/10.1002/esp.3374, 2013.

Krautblatter, M., Weber, S., Dietze, M., Keuschnig, M., Stockinger, G., Brückner, L., Beutel, J., Figl, T., Trepmann, C., Hofmann, R., Rau, M., Pfluger, F., Barbosa Mejia, L., and Siegert, F.: The 2023 Fluchthorn massive permafrost rock slope failure analysed, EGU General Assembly 2024, Vienna, Austria, 14–19 Apr 2024, EGU24-20989, https://doi.org/10.5194/egusphere-egu24-20989, 2024.

Lambrecht, A. and Kuhn, M.: Glacier changes in the Austrian Alps during the last three decades, derived from the new Austrian glacier inventory, Ann. Glaciol., 46, 177–184, https://doi.org/10.3189/172756407782871341, 2007.

Leith, K., Moore, J. R., Amann, F., and Loew, S.: Subglacial extensional fracture development and implications for Alpine Valley evolution, J. Geophys. Res.-Earth, 119, 62–81, 2014.

Lepique, M.: Empfehlung Nr. 10 des Arbeitskreises 3.3 "Versuchstechnik Fels" der Deutschen Gesellschaft für Geotechnik e. V.: Indirekter Zugversuch an Gesteinsproben – Spaltzugversuch, Bautechnik, 85, 623–627, https://doi.org/10.1002/bate.200810048, 2008.

Leroueil, S., Locat, J., Vaunat, J., Picarelli, L., Lee, H., and Faure, R. M.: Geotechnical characterization of slope movements, in: Proceedings of the Seventh International Symposium on Landslides, edited by: Senneset, K., Trondheim, Norway, Balkema, Rotterdam., 53–74, ISBN 9054108185, 1996.

Loke, M. H. and Barker, R. D.: Rapid least-squares inversion of apparent resistivity pseudosections by a quasi-Newton method, Geophys. Prospect., 44, 131–152, 1996.

Magnin, F. and Josnin, J.-Y.: Water Flows in Rock Wall Permafrost: A Numerical Approach Coupling Hydrological and Thermal Processes, J. Geophys. Res.-Earth, 126, e2021JF006394, https://doi.org/10.1029/2021JF006394, 2021.

Magnusson, J., Kobierska, F., Huxol, S., Hayashi, M., Jonas, T., and Kirchner, J. W.: Melt water driven stream and groundwater stage fluctuations on a glacier forefield (Dammagletscher, Switzerland), Hydrol. Process., 28, 823–836, 2014.

Mamot, P., Weber, S., Schröder, T., and Krautblatter, M.: A temperature- and stress-controlled failure criterion for ice-filled permafrost rock joints, The Cryosphere, 12, 3333–3353, https://doi.org/10.5194/tc-12-3333-2018, 2018.

Mamot, P., Weber, S., Lanz, M., and Krautblatter, M.: Brief communication: The influence of mica-rich rocks on the shear strength of ice-filled discontinuities, The Cryosphere, 14, 1849–1855, https://doi.org/10.5194/tc-14-1849-2020, 2020.

Mamot, P., Weber, S., Eppinger, S., and Krautblatter, M.: A temperature-dependent mechanical model to assess the stability of degrading permafrost rock slopes, Earth Surf. Dynam., 9, 1125–1151, https://doi.org/10.5194/esurf-9-1125-2021, 2021.

McColl, S. T.: Paraglacial rock-slope stability, PhD thesis, University of Canterbury, New Zealand, https://doi.org/10.1016/j.geomorph.2012.02.015, 2012.

McColl, S. T. and Davies, T. R. H.: Large ice-contact slope movements: glacial buttressing, deformation and erosion, Earth Surf. Proc. Land., 38, 1102–1115, https://doi.org/10.1002/esp.3346, 2013.

McColl, S. T. and Draebing, D.: Rock slope instability in the proglacial zone: State of the Art, Geomorphology of Proglacial Systems: Landform and Sediment Dynamics in Recently Deglaciated Alpine Landscapes, 119–141, https://doi.org/10.1007/978-3-319-94184-4_8, 2019.

Mellor, M.: Mechanical properties of rocks at low temperatures, in: 2nd International Conference on Permafrost, Yakutsk, 334–344, 1973.

Min, K.-B., Rutqvist, J., Tsang, C.-F., and Jing, L.: Stress-dependent permeability of fractured rock masses: a numerical study, International Journal of Rock Mechanics and Mining Sciences, 41, 1191–1210, https://doi.org/10.1016/j.ijrmms.2004.05.005, 2004.

Mitchell, S. G. and Montgomery, D. R.: Influence of a glacial buzzsaw on the height and morphology of the Cascade Range in central Washington State, USA, Quaternary Res., 65, 96–107, https://doi.org/10.1016/j.yqres.2005.08.018, 2006.

Noetzli, J. and Gruber, S.: Transient thermal effects in Alpine permafrost, The Cryosphere, 3, 85–99, https://doi.org/10.5194/tc-3-85-2009, 2009.

Offer, M., Weber, S., Krautblatter, M., Hartmeyer, I., and Keuschnig, M.: Pressurised water flow in fractured permafrost rocks revealed by joint electrical resistivity monitoring and borehole temperature analysis, EGUsphere [preprint], https://doi.org/10.5194/egusphere-2024-893, 2024.

Oliva, M., Fernández-Fernández, J. M., and Nỳvlt, D.: The Periglaciation of Europe, in: Periglacial Landscapes of Europe, Springer, 477–523, https://doi.org/10.1007/978-3-031-14895-8, 2023.

Pudasaini, S. P. and Krautblatter, M.: A two-phase mechanical model for rock-ice avalanches, J. Geophys. Res.-Earth, 119, 2272–2290, https://doi.org/10.1002/2014JF003183, 2014.

PERMOS: Rock Falls Data Portal, https://www.permos.ch/data-portal/rock-falls, last access: 22 October 2024.

Pettersson, R.: Dynamics of the cold surface layer of polythermal Storglaciären, Sweden – Doctoral dissertation, PhD thesis, Stockholm University, Sweden, ISBN 91-7265-907-6, 2004.

Phillips, M., Wolter, A., Lüthi, R., Amann, F., Kenner, R., and Bühler, Y.: Rock slope failure in a recently deglaciated permafrost rock wall at Piz Kesch (Eastern Swiss Alps), February 2014, Earth Surf. Proc. Land., 42, 426–438, https://doi.org/10.1002/esp.3992, 2017.

Pogrebiskiy, M. I., Chernyshev, S. N., and COLD REGIONS RESEARCH AND ENGINEERING LAB HANOVER NH: Determination of the Permeability of the Frozen Fissured Rock Massif in the Vicinity of the Kolyma Hydroelectric Power Station (Oshenka Vodopronishaemosti Merzlogo Greshinovatogo Massiva Gornkh Porod Uchastka Kolmskoy ges), Cold Regions Research and Engineering Laboratory, Hanover, NH, 1977.

Prager, C., Zangerl, C., Patzelt, G., and Brandner, R.: Age distribution of fossil landslides in the Tyrol (Austria) and its surrounding areas, Nat. Hazards Earth Syst. Sci., 8, 377–407, https://doi.org/10.5194/nhess-8-377-2008, 2008.

Rechberger, C. and Zangerl, C.: Rock mass characterisation and distinct element modelling of a deep-seated rock slide influenced by glacier retreat, Eng. Geol., 300, 106584, https://doi.org/10.1016/j.enggeo.2022.106584, 2022.

Scandroglio, R., Weber, S., Rehm, T., and Krautblatter, M.: An empirically-derived hydraulic head model controlling water storage and outflow over a decade in degraded permafrost rock slopes (Zugspitze, D/A), EGUsphere [preprint], https://doi.org/10.5194/egusphere-2024-1512, 2024.

Shugar, D. H., Jacquemart, M., Shean, D., Bhushan, S., Upadhyay, K., Sattar, A., Schwanghart, W., McBride, S., de van Vries, M. W., and Mergili, M.: A massive rock and ice avalanche caused the 2021 disaster at Chamoli, Indian Himalaya, Science, 373, 300–306, 2021.

Sommer, C., Malz, P., Seehaus, T. C., Lippl, S., Zemp, M., and Braun, M. H.: Rapid glacier retreat and downwasting throughout the European Alps in the early 21st century, Nat. Commun., 11, 3209, https://doi.org/10.1038/s41467-020-16818-0, 2020.

Sommer, C., Fürst, J. J., Huss, M., and Braun, M. H.: Constraining regional glacier reconstructions using past ice thickness of deglaciating areas – a case study in the European Alps, The Cryosphere, 17, 2285–2303, https://doi.org/10.5194/tc-17-2285-2023, 2023.

Stoll, V.: UDEC-Modelling of hydrostatic pressure and its effects on rock slope stability – Case study Hochvogel and Zugspitze (Northern Calcareous Alps, Germany/Austria), unpublished Master's thesis, Technical University of Munich, Chair of Landslide Research, 2020.

Strauhal, T., Zangerl, C., Fellin, W., Holzmann, M., Engl, D. A., Brandner, R., Tropper, P., and Tessadri, R.: Structure, Mineralogy and Geomechanical Properties of Shear Zones of Deep-Seated Rockslides in Metamorphic Rocks (Tyrol, Austria), Rock Mech. Rock Eng., 50, 419–438, https://doi.org/10.1007/s00603-016-1113-y, 2017.

Suter, S.: Cold firn and ice in the Monte Rosa and Mont Blanc areas: spatial occurrence, surface energy balance and climatic evidence, PhD thesis, ETH Zurich, Switzerland, https://doi.org/10.3929/ethz-a-004288434, 2002.

Svennevig, K., Dahl-Jensen, T., Keiding, M., Merryman Boncori, J. P., Larsen, T. B., Salehi, S., Munck Solgaard, A., and Voss, P. H.: Evolution of events before and after the 17 June 2017 rock avalanche at Karrat Fjord, West Greenland – a multidisciplinary approach to detecting and locating unstable rock slopes in a remote Arctic area, Earth Surf. Dynam., 8, 1021–1038, https://doi.org/10.5194/esurf-8-1021-2020, 2020.

Walter, F., Amann, F., Kos, A., Kenner, R., Phillips, M., de Preux, A., Huss, M., Tognacca, C., Clinton, J., Diehl, T., and Bonanomi, Y.: Direct observations of a three million cubic meter rock-slope collapse with almost immediate initia-

tion of ensuing debris flows, Geomorphology, 351, 106933, https://doi.org/10.1016/j.geomorph.2019.106933, 2020.

Welkner, D., Eberhardt, E., and Hermanns, R. L.: Hazard investigation of the Portillo Rock Avalanche site, central Andes, Chile, using an integrated field mapping and numerical modelling approach, Eng. Geol., 114, 278–297, 2010.

Witherspoon, P. A., Wang, J. S., Iwai, K., and Gale, J. E.: Validity of cubic law for fluid flow in a deformable rock fracture, Water Resour. Res., 16, 1016–1024, 1980.

Woo, M.-k.: Permafrost Hydrology, Springer Berlin Heidelberg, Berlin, Heidelberg, ISBN 978-3-642-23461-3, https://doi.org/10.1007/978-3-642-23462-0, 2012.

Zangerl, C., Evans, K. F., Eberhardt, E., and Loew, S.: Normal stiffness of fractures in granitic rock: A compilation of laboratory and in-situ experiments, Int. J. Rock Mech. Min., 45, 1500–1507, https://doi.org/10.1016/j.ijrmms.2008.02.001, 2008.

Zangerl, C., Fey, C., and Prager, C.: Deformation characteristics and multi-slab formation of a deep-seated rock slide in a high alpine environment (Bliggspitze, Austria), B. Eng. Geol. Environ., 78, 6111–6130, https://doi.org/10.1007/s10064-019-01516-z, 2019.